SYNTHESIS, CHARACTERIZATION, AND MOLECULAR MODELING OF VANADIUM COMPLEXES WITH TRIETHYLENETETRAAMINEHEXAACETATE AND PYRIDINEDIMETHANOLATE LIGANDS

By

Zachary N. Pickett

RECOMMENDED:

Brian T. Rasley

Dr. Brian T. Rasley

Dr. John W. Keller

William Howard

Dr. William A. Howard, Advisory Committee Chair

Dr. William R. Simpson, Department of Chemistry and Biochemistry Chair

APPROVED:

Paul W. Layer

Dean Paul W. Layer, Dean College of Natural Science and Mathematics

Lawrence K. Duffy

Dr. Lawrence K. Duffy, Dean of the Graduate School

July 27, 2012

Date

SYNTHESIS, CHARACTERIZATION, AND MOLECULAR MODELING OF VANADIUM COMPLEXES WITH TRIETHYLENETETRAAMINEHEXAACETATE AND PYRIDINEDIMETHANOLATE LIGANDS

A

THESIS

Presented to the Faculty

of the University of Alaska Fairbanks

in Partial Fulfillment of the Requirements

for the Degree of

MASTER OF SCIENCE

By

Zachary N. Pickett, B.S.

Fairbanks, AK

August 2012

Abstract

Sodium triethylenetetraaminehexaacetatodi [oxovanadate(IV)] octahydrate ($Na_2[(V^{IV}O)_2(ttha)] \cdot 8\ H_2O$) has been isolated and characterized spectroscopically and by single crystal X-ray diffraction. This complex was also modeled by density functional theory (DFT), and the spectroscopic data are interpreted in light of the DFT results. Additionally, the complexes $Na[VO_2(pydim\text{-}X)]$ (pydim-X = 4-X-2,6-pyridinedimethanolate; X = H, Cl, NMe_2) and $Na[VO_2(dipic)]$ (dipic = 2,6-pyridinedicarboxylate) were isolated and characterized. The relative stabilities of these complexes were assessed by monitoring reactions between each vanadium complex and either H_2pydim-X or H_2dipic by ^{1}H NMR spectroscopy. The order of relative stability, from the least stable to the most stable, goes as: $[VO_2(pydim\text{-}Cl)]^- < [VO_2(pydim)]^- < [VO_2(pydim\text{-}NMe_2)]^- < [VO_2(dipic)]^-$. Moreover, when $Na[VO_2(pydim\text{-}Cl)]$ and $Na[VO_2(pydim\text{-}NMe_2)]$ are decomposed in acidic solution, the protonated ligands $[H_3pydim\text{-}Cl]^+Cl^-$ and $[(H_3pydim\text{-}NMe_2)Cl]_2(H_2O)$ are obtained. These protonated ligands were structurally characterized by single crystal X-ray diffraction.

Table of Contents

Page

List of Figures

Page

List of Tables

Page

Abbreviations

ttha ..... Triethylenetetramine-N,N,N',N',N'',N''-hexaacetate ion

edta..... Ethylenediamine-N,N,N',N'-tetraacetate ion

DFT..... Density Functional Theory

TDDFT..... Time-Dependent Density Functional Theory

edda..... Ethylenediamine-N,N'-diacetate ion

HOMO ..... highest occupied molecular orbital

LUMO..... lowest unoccupied molecular orbital

pydim 2,6-pyridinedimethanolate

dipic 2,6-pyridinedicarboxylate

dipic-OH 4-hydroxy-2,6-pyridinedicarboxylate

pydim-Cl 4-chloro-2,6-pyridinedimethanolate

pydim-NMe_2..... 4-dimethylamino-2,6-pyridinedimethanolate

Acknowledgements

I would like to thank the Department of Chemistry & Biochemistry for financial support for my research, and the National Science Foundation for their support (CHE-0619638) for the purchase of the X-ray diffractometer at Columbia University which made the research discussed in Chapter 2 possible. I would also like to thank the National Science Foundation for their support (DUE-9850731) in the purchase of the 300 MHz NMR which made the research discussed in Chapter 3 possible.

The X-ray structures of $[H_3pydim\text{-}Cl]^+Cl^-$ and $[H_3pdyim\text{-}NMe_2]^+Cl^-$ were obtained by Dr. Christopher Graves, a postdoctoral fellow at Los Alamos National Laboratory, and by Dr. William Howard Associate Professor of Chemistry at the University of Alaska Fairbanks, respectively. The X-ray structure of $Na_2[(VO)_2(ttha)](H_2O)_8$ was obtained by Keliang Pang, a PhD student at Columbia University. Dr. John Keller, Professor of Chemistry at the University of Alaska Fairbanks, and Dr. Greg Cushing, Ph.D. University of Virginia, assisted in the optimization of the DFT calculated structures. Dr. John Keller performed the final optimization on $[(VO)_2(ttha)]^{2-}$. Dr. Michael Goldfeld obtained the electron spin resonance spectrum of $Na_2[(VO)_2(ttha)] \cdot 8H_2O$. Special thanks would like to be given to the Arctic Regional Supercomputing Facility for the use of the computing resources for the computational aspects within this thesis.

Chapter 1 General Introduction

1.1 Introduction

As of 2004, Diabetes (*diabetes mellitus*) affected 140 million people worldwide [1]. Insulin, a hormone that is produced in the pancreas, was isolated in 1922 at the University of Toronto. Today insulin is the most accepted treatment for diabetes. Since insulin is degraded in the stomach, diabetic patients must inject the insulin directly into the bloodstream. Insulin treatment also has several other drawbacks. First of all, insulin must be stored in a cool area for optimal life. Insulin at ambient temperatures generally has a life of 28 days whereas unopened insulin stored near 3 °C can last up to two years. Temperature extremes can destroy the hormone, this includes freezing. If insulin is injected at cool stable temperatures, more discomfort is noticed than insulin injected at room temperature, and thus insulin may be heated above optimal conditions to inject comfortably.

Much research over the last few decades has been devoted towards the development a less invasive and more convenient method for treating diabetes. One possible alternative to insulin treatment is to use vanadium based compounds, which may offer an orally administered treatment.

Vanadium itself has been used to treat diabetes since 1899, when Dr. Lyonett treated 60 diabetes patients with sodium metavanadate [2]. The diabetic patients consumed 4-5 mg of the salt three times a week before meals. A slight decrease in blood glucose levels

were observed, without any noted side effects. After the discovery of insulin in 1922, interest in vanadium treatment faded. Instead vanadium compounds were examined for their ability to control serum cholesterol [3-5]. In the mid 1970s continued research revealed that vanadium can inhibit (sodium+potassium)-ATPase [6].

As interest in the bio-significance of vanadium compounds grew, research was directed at glucose metabolism studies. By the late 1970s and early 1980s research confirmed that vanadium can play a significant role in the oxidation of glucose [7-10]. In 1985 a breakthrough in vanadium treatment for diabetes occurred when an *in vivo* study involving streptozotocin-induced diabetic rats were treated with sodium orthovanadate [11]. This study was a model for many others that followed, and illustrated even dilute solutions of vanadium can play a key role in controlling diabetes.

To date, a wide variety of vanadium compounds have shown the ability to lower blood glucose levels. For example, vanadium compounds with oxidation states of (III), (IV), and (V) have been effective potential drugs [12-14]. Inorganic and organic vanadium compounds, along with compounds with four, five, six and seven coordination numbers have also been successful [11, 14]. Even cationic and anionic compounds are viable options for insulin-mimetic drugs [12, 14, 15].

Though inorganic and organic compounds have been shown to lower glucose levels, compounds with chelating organic ligands have been the most successful. These organic compounds are more effectively absorbed into the gastrointestinal tract [16, 17]. Studies

have shown after 24 hours 75% of vanadyl sulfate is removed in the feces compared to 62% of Bis(maltolato)oxovanadium(IV) [18].

Though vanadium compounds have been successful at lowering glucose levels in diabetic patients, the toxicity of these compounds has prevented wide spread use. These vanadium compounds have been found to incorporate into the bones and organs of streptozotocin -induced diabetic rats [19, 20]. A recent study looking at Bis(picolinato)oxovanadium(IV), considered to be one of the most potent insulin-mimetic vanadium complexes, showed that when vanadium is incorporated into the bones and organs, the complex must first be completely decomposed [21].

Along with being absorbed more readily, chelating organic complexes have shown higher toxicities than the inorganic group of complexes [18, 22]. Bis(maltolato)oxovanadium(IV) for example accumulates in the bone and organ tissue 1.4-4 times the rate of vanadyl sulfate depending on the tissue [18].

One possible explanation for the accumulation of vanadium in these regions of the body is the influence of serum proteins [18]. Transferrin and albumin for example have a strong affinity for vanadium and have been shown to displace the organic ligands [23]. Since little is known on how the vanadium compounds facilitate the insulin-mimetic properties, understanding the interactions between the vanadium compounds and serum proteins are increasingly important. Transferrin has been modeled by several chelating ligands in the past, however each have had their drawbacks [6, 7]. Transferrin itself is an 80 kilodalton protein with two active sites vanadium can bind to [24]. The vanadium

center exists as vanadium (IV), and the geometry is octahedral [18, 24]. A realistic model would incorporate dual binding sites, the correct oxidation state of vanadium, and an octahedral geometry. Triethylenetetramine-N,N,N',N',N'',N''-hexaacetic acid (ttha) is a molecule that exhibits all of the above features. Though vanadium has successfully been coordinated to ttha in the past, it has never been proposed as a model for the transferrin-vanadium complex.

Along with understanding the interaction of these serum proteins with vanadium based molecules, understanding how successfully various organic ligands bind to the vanadium center is key to developing a useful drug. If the various serum proteins' affinity for vanadium is influential in the buildup of vanadium in bone and organ tissues, than a drug which possesses ligands that coordinate to the vanadium center strong enough to remain stable in the presence of these serum proteins may reduce these negative side effects.

Based on vanadium's unique chemistry in the body, there are several properties that are required to design a successful orally administered drug. First the compound must be stable in the stomach where pH values are between 1-2. Next the compound should be stable in blood pH ranges and in the presence of serum proteins. Finally the drug must be readily absorbed in the gastrointestinal tract.

Research over the last two years has been aimed at designing an effective vanadium-transferrin model. The work contained in chapter one presents the idea of using a vanadium-ttha complex as a suitable model. Though dinuclear vanadium-ttha

compounds have been formed the sodium analog of these compounds has previously not been synthesized. Synthesis and characterization of the novel compound $Na_2[(VO)_2(ttha)] \cdot 8\ H_2O$ is presented in chapter one along with pH and thermal stability studies.

Also during this time 4-substituted 2,6-pyridinedimethanol ligands were developed and their stabilities were evaluated relative to each other. The goal of this study was to examine how electron donating or withdrawing groups influence the stabilities of the ligands coordinated to vanadium.

1.2 References

1. K. V. Larin, T. V. Ashitkov, M. Motamedi, R. O. Esenaliev, Proc. SPIE-Int. Soc. Opt. Eng. 5068 (2003), 294.
2. K. H. Thompson, C. Orvig, J. Inorg. Biochem. 100 (2006) 1925.
3. G. L. Curran, D. L. Azarnoff, R. E. Bolinger, J. of Clin. Invest. 38 (1959) 1251.
4. J. Somerville, B. Davies, Am. Heart J. 64 (1962) 54.
5. E. G. Dimond, J. Caravaca, A. Benchimol, Am. J. of Clin. Nutr. 12 (1963) 49.
6. S. J. D. Karlish, L. A. Beauge, I. M. Glynn, Nature (London, United Kingdom), 282 (1979) 333.
7. H. Degani, M. Gochin, S. J. D. Karlish, Y. Shechter, Biochem. 20 (1981) 5795.
8. P. Ninfali, A. Accorsi, A. Fazi, F. Palma, G. Fornaini, Arch Biochem. Biophys. 226 (1983) 441.
9. S. Tamura, T. A. Brown, R. E. Dubler, J. Larner, Biochem. and Biophys. Res. Commun. 113 (1983) 80.
10. E. L. Tolman, E. Barris, M. Burns, A. Pansini, R. Partridge, Life Sci. 25 (1979) 1159.
11. C. E. Heyliger, A. G. Tahiliani, J. H. McNeill, Sci. 227 (1985) 1474.
12. P. Buglyo, D. C. Crans, E. M. Nagy, R. L. Lindo, L. Yang, J. J. Smee, W. Jin, L.-H. Chi, M. E. Godzala, III, G. R. Willsky, Inorg. Chem. 44 (2005) 5416.
13. S. Bhanot, M. Bryer-Ash, A. Cheung, J. H. McNeill, Diabetes 43 (1994) 857.

14. D. C. Crans, M. Mahroof-Tahir, M. D. Johnson, P. C. Wilkins, L. Yang, K. Robbins, A. Johnson, J. A. Alfano, M. E. Godzala, L. T. Austin, G. R. Willsky, Inorg. Chim. Acta 356 (2003) 365.

15. S. M. Brichard, W. Okitolonda, J. C. Henquin, Endocrin. 123 (1988) 2048.

16. K. H. Thompson, C. Orvig, J. Chem. Soc., Dalton Trans. (2000), 2885.

17. V. G. Yuen, C. Orvig, J. H. McNeill, Can. J. Physiol. Pharmacol. 71 (1993) 263.

18. I. A. Setyawati, K. H. Thompson, V. G. Yuen, Y. Sun, M. Battell, D. M. Lyster, C. Vo, T. J. Ruth, S. Zeisler, J. H. McNeill, C. Orvig, J. Appl. Physiol. 84 (1998) 569.

19. S. Fujimoto, K. Fujii, H. Yasui, R. Matsushita, J. Takada and H. Sakurai, J. Clin. Biochem. Nutr. 23 (1997) 113.

20. S. Dai, K. H. Thompson, E. Vera, J. H. McNeill, Pharmacol. Toxicol. 75 (1994) 265.

21. K. Fukui, Y. Fujisawa, H. OhyaNishiguchi, H. Kamada, H. Sakurai, J. Inorg. Biochem. 77 (1999) 215.

22. T. Takino, H. Yasui, A. Yoshitake, Y. Hamajima, R. Matsushita, J. Takada, H. Sakurai, J. Biol. Inorg. Chem. 6 (2001) 133.

23. E. Sabbioni, E. Marafante, L. Amantini, L. Ubertalli, C. Birattari, Bioinorg. Chem. 8 (1978) 503.

24. C.E. Housecroft, A.G. Sharpe, *Inorganic Chemistry 3rd ed.*; Prentice Hall, 2007.

Chapter 2 Spectroscopic and Structural Characterization of $Na_2[(VO)_2(ttha)] \cdot 8 H_2O$; Interpreting the Results with Density Functional Theory[1]

2.1 Introduction

The X-ray structures of several compounds containing $[(V^{IV}O)_2(ttha)]^{2-}$ have been reported [1 – 4], and the magnetic and spectroscopic properties of some of these compounds have been described in detail [1]. This complex ion consists of two seemingly independent (VO)(edta)-like moieties linked through an ethylene tether. Our initial interest in $[(VO)_2(ttha)]^{2-}$ stemmed from the notion that this compound may serve as a model of the vanadium – transferrin complex [5 – 16]. The transferrin-vanadium complex has been modeled in the past, but each model has differed from transferrin in some notable respect. For instance, one molecule of transferrin can bind two vanadium atoms, but the model $[(V^{IV}=O)$(N,N'-*bis*(2-hydroxybenzyl)-N,N'-*bis*(2-pyridylmethyl)ethylenediamine)] is mononuclear [17]. Moreover, transferrin has been shown to bind vanadium (IV) preferentially over vanadium (V), yet the dinuclear model $(NH_4)_2[V(OC(CH_2CH_3)_2COO)(O)_2]_2$ features vanadium (V) and not vanadium (IV) [18]. A better transferrin-vanadium model complex would be dinuclear and would feature vanadium (IV) ions. Vanadyl complexes of the triethylenetetraamine-N,N,N',N'',N''',N'''-hexaacetate ion (ttha) exhibit both of these features, yet vanadyl-ttha complexes have never been proposed as models for the transferrin-vanadium complex.

---

[1] Z.N. Pickett, W.A. Howard, K. Pang, Polyhedron. 29 (2010) 521.

Before beginning our modeling studies however, we sought a better understanding of the spectroscopic and electronic properties of $[(VO)_2(ttha)]^{2-}$ by carrying out DFT calculations. In this thesis, a new synthesis of $Na_2[(VO)_2(ttha)] \cdot 8\ H_2O$ is described, as well as the X-ray structure and some spectroscopic characteristics. Furthermore, the anion $[(VO)_2(ttha)]^{2-}$ was modeled by DFT and TDDFT. The computational results are used to interpret the actual structural and spectroscopic data.

2.2 Results

As summarized in Figure 2.1, triethylenetetraamine-N, N, N', N", N'", N'"-hexaacetic acid (H_6ttha) reacts with three equivalents of vanadyl(IV) acetate in aqueous solution at 55°C to yield pentaaquooxovanadium(IV) triethylenetetraaminehexaacetatodi [oxovanadate(IV)] tetrahydrate ($[VO(H_2O)_5][(VO)_2(ttha)] \cdot 4\ H_2O$), a royal blue complex previously described as the product from the reaction between H_6ttha and vanadyl(IV) sulfate at 150°C [1]. This was verified by obtaining a structure using single crystal X-ray diffraction. Since the structure obtained was identical to the data reported previously, the single crystal X-ray diffraction data was not presented for this compound. Reacting H_6ttha with two equivalents of vanadyl(IV) acetate in water at 55°C produces a mixture of $[VO(H_2O)_5][(VO)_2(ttha)] \cdot 4\ H_2O$ and unreacted H_6ttha, which was verified by comparing the UV-Vis spectra.

Figure 2.2 summarizes the synthesis of the blue sodium salt $Na_2[(VO)_2(ttha)] \cdot 8\ H_2O$, which is conveniently prepared by titrating an aqueous suspension of H_6ttha with six equivalents of NaOH (aq), followed by reaction two equivalents of

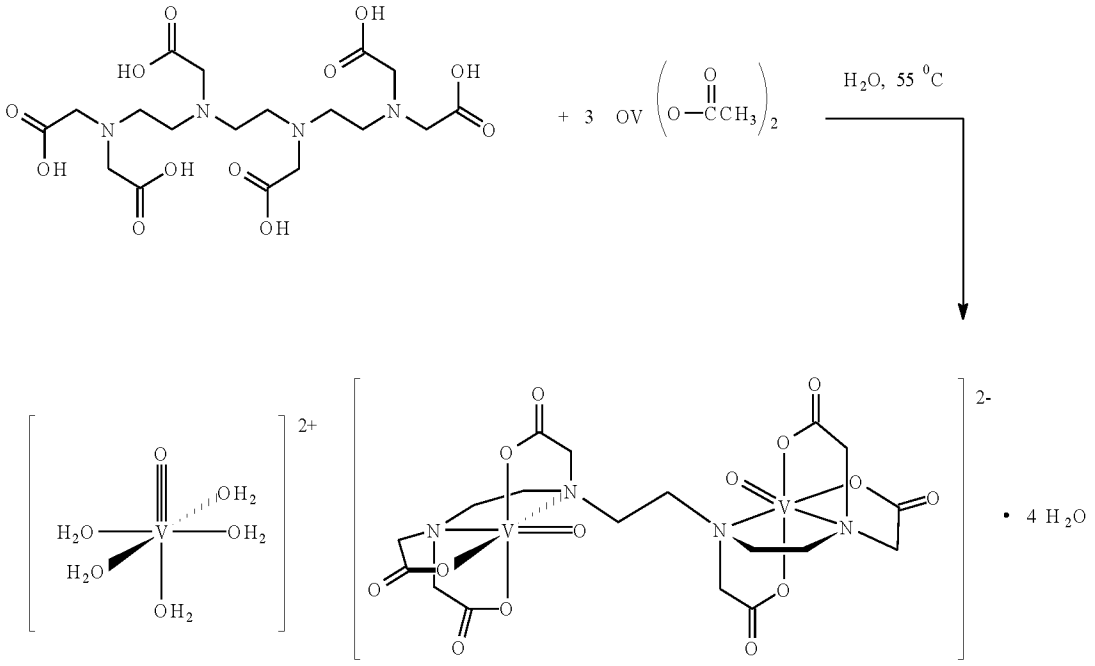

Figure 2.1. Synthesis of $[(H_2O)_5VO][(VO)_2(ttha)] \cdot 4\ H_2O$.

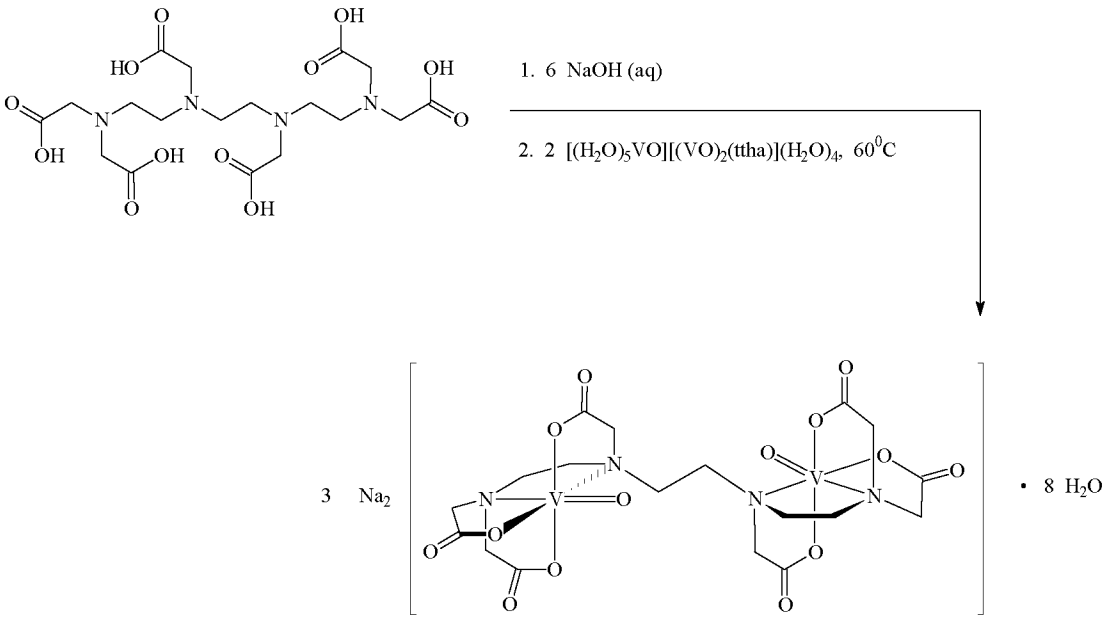

Figure 2.2. Synthesis of $Na_2[(VO)_2(ttha)] \cdot 8\ H_2O$.

$[VO(H_2O)_5][(VO)_2(ttha)] \cdot 4\ H_2O$ at 60°C. This straightforward synthesis contrasts with a previously published procedure for making the potassium analog, $K_2[(VO)_2(ttha)] \cdot 6\ H_2O$, which involved treating NH_4VO_3 with five equivalents of H_6ttha, malic acid, and KOH in aqueous solution at 85°C [2]. Apart from losing the eight associated water molecules, solid $Na_2[(VO)_2(ttha)] \cdot 8\ H_2O$ is stable at 100°C under vacuum for at least one day, and an aqueous solution of $Na_2[(VO)_2(ttha)] \cdot 8\ H_2O$ is also stable at 100°C for at least one week.

2.3 X-Ray Structure of $Na_2[(VO)_2(ttha)] \cdot 8\ H_2O$

$Na_2[(VO)_2(ttha)] \cdot 8\ H_2O$ was structurally characterized by single crystal X-ray diffraction. A thermal ellipsoid plot is shown in Figure 2.3, and the crystal and structural refinement data are summarized in Table A1 in the Appendix. Selected bond lengths and bond angles for $Na_2[(VO)_2(ttha)] \cdot 8\ H_2O$ are compared with those of the previously published X-ray structures of $Na_2[(VO)_2(ttha)] \cdot 6\ H_2O$ [3], $Na_2[(VO)_2(ttha)] \cdot 10\ H_2O$ [4], $[(H_2O)_5VO][(VO)_2(ttha)] \cdot 4\ H_2O$ [1], and $K_2[(VO)_2(ttha)] \cdot 6\ H_2O$ [2] in Table 2.1. Moreover, the dianion $[(VO)_2(ttha)]^{2-}$ was modeled by DFT calculations, and the calculated bond lengths and angles are also included in Table 2.1 for comparison. The DFT calculated atomic coordinates and total energy can be found in Table A2 of the Appendix.

For the most part, there is little variation in the structures of the $[(VO)_2(ttha)]^{2-}$ anions among $Na_2[(VO)_2(ttha)] \cdot 8\ H_2O$, $Na_2[(VO)_2(ttha)] \cdot 6\ H_2O$, $Na_2[(VO)_2(ttha)] \cdot 10$

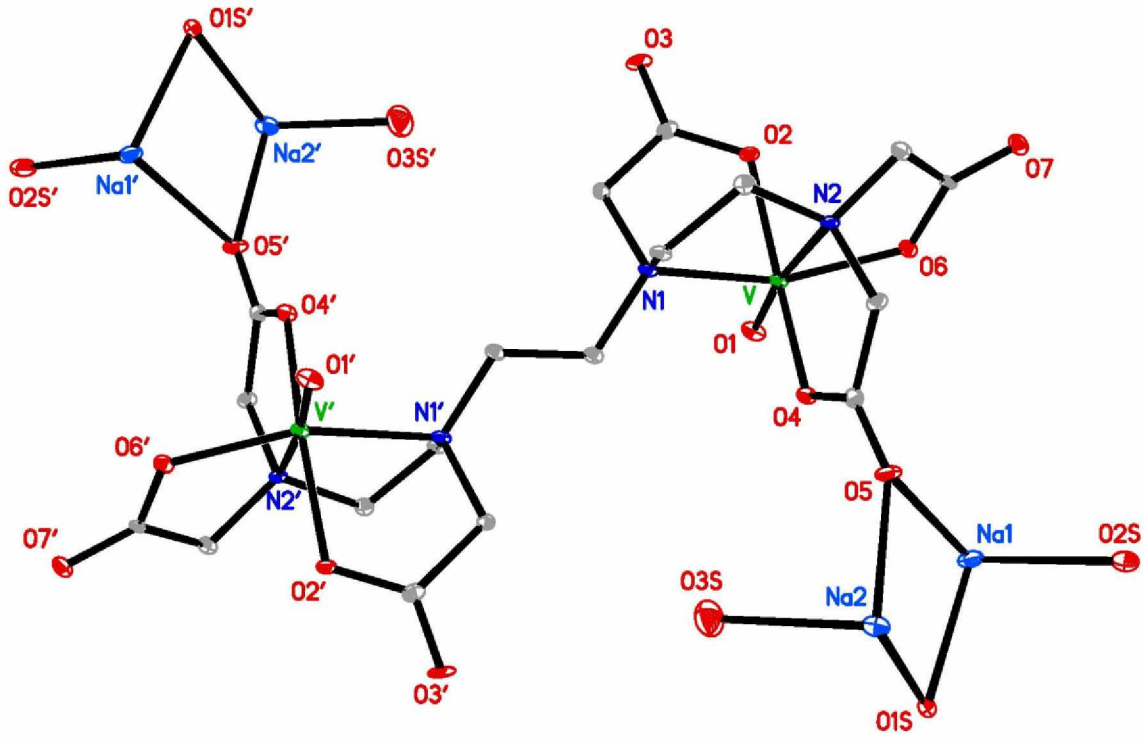

Figure 2.3. Thermal Ellipsoid Plot of $Na_2[(VO)_2(ttha)] \cdot 8\ H_2O$.

H_2O, $[VO(H_2O)_5][(VO)_2(ttha)] \cdot 4\ H_2O$, and $K_2[(VO)_2(ttha)] \cdot 6\ H_2O$. For each structure, there exists a center of inversion in $[(VO)_2(ttha)]^{2-}$, and both vanadium centers possess a pseudooctahedral coordination geometry. The [V = O] bond distance of 1.595(3) Å in $Na_2[(VO)_2(ttha)] \cdot 8\ H_2O$ is typical [19] and compares favorably with those in the other structures shown in Table 2.1. The [V – N(2)] bond distance is consistently longer by *ca.* 0.1 to 0.15 Å than the [V – N(1)] distance in all five X-ray structures presented in Table 2.1, and this same observation is made for the DFT calculated structure as well. The N(2) atom is *trans* to the terminal oxo ligand, while the N(1) atom is *trans* to a carboxylate oxygen atom. The longer [V – N(2)] bond distance is simply a consequence of the stronger *trans* influence of the oxo ligand versus the carboxylate oxygen atom. A similar situation in which one nitrogen atom is *trans* to a terminal oxo ligand and the

other nitrogen atom is *trans* to a carboxylate oxygen atom is found in the X-ray structures of β-*cis*-$NH_4[VO_2(edda)]$ [20], Ba(VO)(edta) [21], Na(VO)(edtaH) · 4 H_2O [22], $Na_3[VO_2(edta)] \cdot 4\ H_2O$ [23], and $NH_4[VO_2(edtaH_2)] \cdot 3\ H_2O$ [24]. As in the case with $[(VO)_2(ttha)]^{2-}$, the V – N bond distance, where the nitrogen atom is *trans* to the terminal oxo ligand, is longer by *ca.* 0.1 to 0.15 Å than the V – N bond distance, where the

Table 2.1. A Comparison of Selected Bond Lengths (Å) and Angles (degrees) from the Actual X-Ray Structures of $Na_2[(VO)_2(ttha)] \cdot 8\ H_2O$,[(a)] $Na_2[(VO)_2(ttha)] \cdot 6\ H_2O$,[(b)] $Na_2[(VO)_2(ttha)] \cdot 10\ H_2O$,[(c)] $[(H_2O)_5VO][(VO)_2(ttha)] \cdot 4\ H_2O$,[(d)] and $K_2[(VO)_2(ttha)] \cdot 6\ H_2O$,[(e)] and the DFT Calculated Structure of the $[(VO)_2(ttha)]^{2-}$ Ion.[(a)]

Bond Length or Angle	DFT Calculated Structure	$Na_2[(VO)_2(ttha)] \cdot 8\ H_2O$	$Na_2[(VO)_2(ttha)] \cdot 6\ H_2O$	$Na_2[(VO)_2(ttha)] \cdot 10\ H_2O$	$[(H_2O)_5VO][(VO)_2(ttha)] \cdot 4\ H_2O$	$K_2[(VO)_2(ttha)] \cdot 6\ H_2O$
V = O(1)	1.59761	1.595(3)	1.618(3)	1.605(8)	1.610(2)	1.603(2)
V – N(1)	2.26651	2.157(4)	2.174(4)	2.163(5)	2.177(3)	2.162(2)
V – N(2)	2.41121	2.291(4)	2.289(4)	2.294(7)	2.278(3)	2.290(2)
V – O(6)	1.89615	2.013(3)	1.993(3)	2.006(5)	1.999(2)	2.003(2)
V – O(4)	1.90313	2.016(3)	2.001(3)	1.986(4)	1.994(2)	2.004(2)
V – O(2)	1.90834	1.998(3)	1.998(3)	1.986(4)	1.989(2)	1.989(2)
O(5) – Na(1)		2.401(3)	2.561(6)	2.356		
Na(1) – O(2S)		2.415(4)	2.366(4)	2.455		
O(1) – V – N(1)	105.068	102.63(15)	101.2(1)		100.47(11)	101.61(8)
O(1) – V – N(2)	174.405	171.10(15)	172.1(2)	172.5(3)	174.14(12)	172.70(7)
O(1) – V – O(6)	102.343	103.22(15)	104.2(2)		105.45(11)	104.46(8)
O(1) – V – O(2)	99.7311	103.35(14)	102.0(2)		102.25(12)	102.74(7)
O(1) – V – O(4)	101.156	95.38(14)	95.5(2)		96.67(12)	95.29(7)
N(1) – V – N(2)	77.4262	80.65(13)	80.4(1)	80.2(2)	79.96(9)	80.18(6)
N(1) – V – O(2)	88.6019	80.66(13)	80.8(1)	80.5(2)	80.09(10)	80.50(6)
N(1) – V – O(6)	151.960	153.39(13)	154.0(1)	153.5(2)	153.04(10)	152.90(6)
N(1) – V – O(4)	79.8404	89.27(13)	88.1(1)		89.25(10)	91.74(6)
N(2) – V – O(2)	75.1937	85.29(13)	85.9(1)		83.60(10)	84.82(6)
N(2) – V – O(6)	75.8108	74.72(13)	75.1(1)	94.0(2)	75.01(9)	74.96(6)
N(2) – V – O(4)	84.1640	76.29(12)	76.8(1)	76.8(2)	77.48(9)	77.23(6)
O(6) – V – O(2)	92.5355	87.38(13)	88.7(1)		87.27(10)	86.61(6)
O(6) – V – O(4)	89.2439	94.47(12)	94.6(1)		94.9(1)	93.14(6)
O(2) – V – O(4)	158.144	160.25(12)	160.8(1)	159.7(2)	159.66(10)	161.45(6)

(a) This work; (b) Reference 3; (c) Reference 4; (d) Reference 1; (e) Reference 2

nitrogen atom is *trans* to a carboxylate oxygen atom, in the structures of β-*cis*-$NH_4[VO_2(edda)]$, Ba(VO)(edta), and Na(VO)(edtaH) · 4 H_2O. In contrast however, the two V – N bond lengths in $Na_3[VO_2(edta)] \cdot 4\ H_2O$ (2.359(2) vs. 2.366(2) Å) and in $NH_4[VO_2(edtaH_2)] \cdot 3\ H_2O$ (2.351(2) vs. 2.362(3) Å) are effectively the same, despite the fact that one nitrogen atom is *trans* to an oxo ligand while the other is *trans* to a carboxylate group. Moreover, the two V – N bonds in $Na[V(edta)(H_2O)] \cdot 3\ H_2O$, which has no terminal oxo ligands, are in chemically similar environments, and the bond distances are very close (2.225(2) and 2.217(3) Å) [25].

There is at least one significant difference, however, among the structures of the $[(VO)_2(ttha)]^{2-}$ anions of the different compounds represented in Table 2.1. While the N(2) – V – O(6) bond angle is about 74 or 75° in four of the structures in Table 2.1, this bond angle is reported to be 94.0(2)° in $Na_2[(VO)_2(ttha)] \cdot 10\ H_2O$ [4]. For comparison, the DFT calculated N(2) – V – O(6) bond angle is 75.81°.

A second thermal ellipsoid plot shown in Figure 2.4 reveals the coordination geometry of the sodium ions in $Na_2[(VO)_2(ttha)] \cdot 8\ H_2O$. Each sodium ion in $Na_2[(VO)_2(ttha)] \cdot 8\ H_2O$ is six-coordinate, bonded with two bridging carboxylate oxygen atoms, two bridging water molecules, and two terminal water molecules. Moreover, there are two additional water molecules per $Na_2[(VO)_2(ttha)]$ formula unit that are hydrogen bonded to carboxylate oxygen atoms, bringing the total number of water molecules to eight per $Na_2[(VO)_2(ttha)]$ formula unit. The [Na(1) – Na(2)] distance in $Na_2[(VO)_2(ttha)] \cdot 8\ H_2O$ is 3.348 Å. Interestingly, the coordination environment of the

sodium ions in $Na_2[(VO)_2(ttha)] \cdot 8\ H_2O$ is not the same as that in $Na_2[(VO)_2(ttha)] \cdot 6\ H_2O$ [3], where one sodium ion is five-coordinate and the other is six-coordinate.

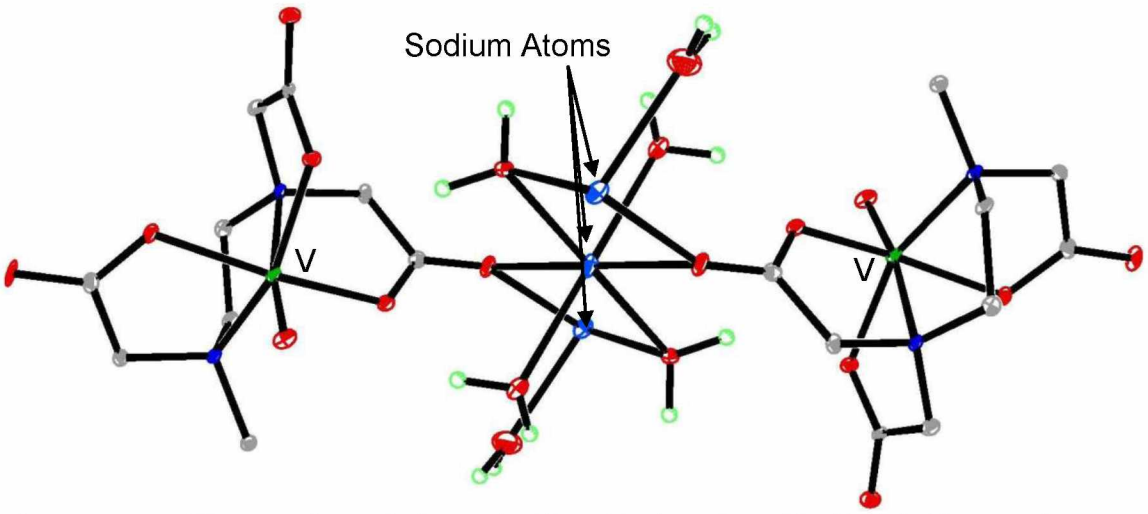

Figure 2.4. Different View of Thermal Ellipsoid Plot of $Na_2[(VO)_2(ttha)] \cdot 8\ H_2O$, Showing the Octahedral Coordination Environment of the Sodium Cation.

In general, there is an overall agreement in the selected bond lengths and angles between the DFT calculated structure and the five experimental X-ray structures. There are some notable differences however. For example, the calculated [V – N(1)] and [V – N(2)] bond distances are > 0.1 Å longer than the actual [V – N(1)] and [V – N(2)] bond distances in all five of the X-ray structures. The calculated [V – O(carboxylate)] bond distances are consistently *ca.* 0.1 Å shorter than the actual [V – O(carboxylate)] bond distances. Moreover, some of the calculated bond angles differ significantly from the actual bond angles. As an example, the calculated [N(1) – V – O(4)] bond angle of 79.8404° is *ca.* 10° lower than the actual [N(1) – V – O(4)] bond angle in each of the five structures. It should be noted that overall agreement between the DFT-calculated

structure and the actual X-ray structure has been reported for some other dinuclear oxovanadium complexes as well [26].

2.4 Infrared Spectrum of $Na_2[(VO)_2(ttha)] \cdot 8\ H_2O$

The actual infrared spectrum of $Na_2[(VO)_2(ttha)] \cdot 8\ H_2O$ and a DFT calculated infrared spectrum of $[(VO)_2(ttha)]^{2-}$ are shown together in Figure 2.5, and the calculated absorption frequencies and their assignments are summarized in Table 2.2. The overall shapes of the calculated and actual spectra are similar, and some peaks in the actual

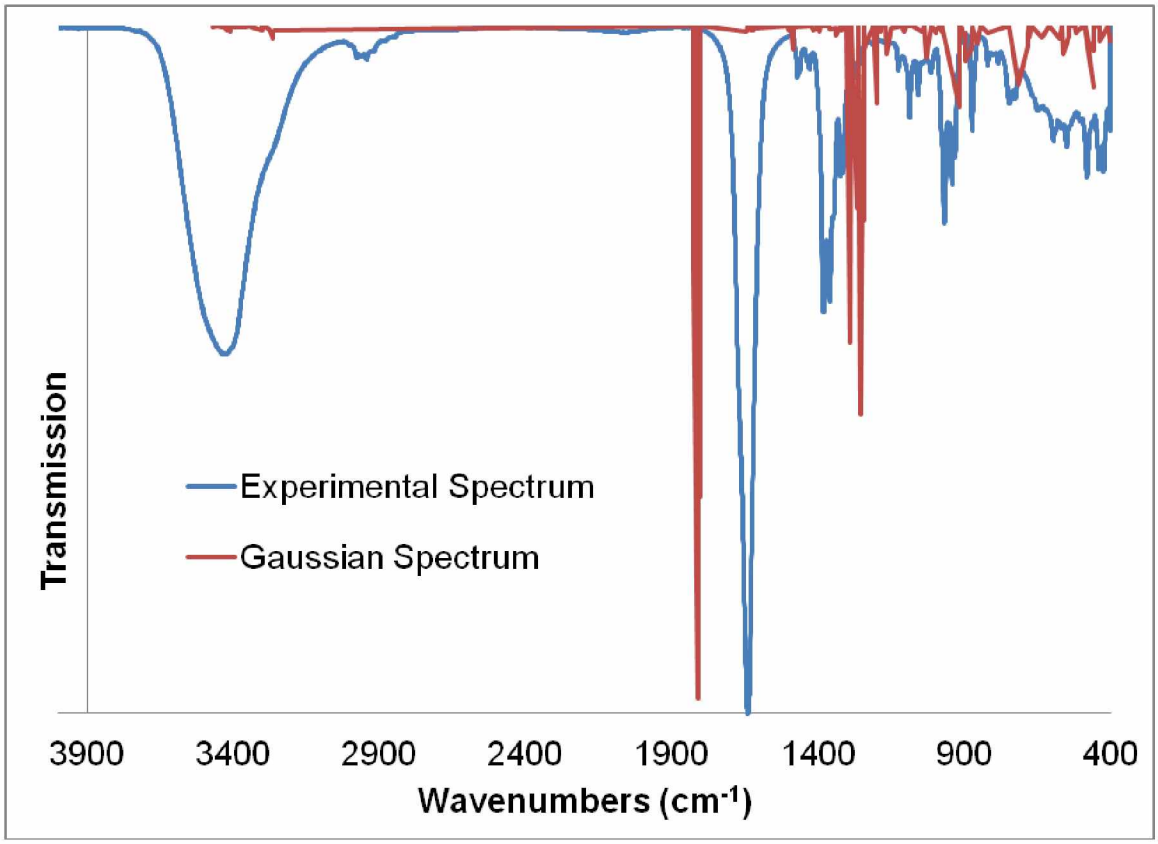

Figure 2.5. Experimental Infrared Spectrum of $Na_2[(VO)_2(ttha)] \cdot 8\ H_2O$ and Calculated Infrared Spectrum of $[(VO)_2(ttha)]^{2-}$.

spectrum can be assigned based on visual comparison with the calculated spectrum. For instance, visual comparison of the two spectra implies that the very strong peak at 1812 cm^{-1} in the calculated spectrum corresponds with the very strong peak at 1641 cm^{-1} in the

Table 2.2. DFT Calculated Infrared Absorptions and Peak Assignments for $[(VO)_2(ttha)]^{2-}$

Absorption (cm^{-1}) and Peak Assignment	Absorption (cm^{-1}) and Peak Assignment
3415 (w, C – H stretch)	1107 (w, C – C stretch)
3267 (w, C – H stretch)	1045 (w, C – C stretch)
1826 (m, C = O stretch)	1029 (w, C – C stretch)
1812 (vs, C = O stretch)	997 (w, H – C – H twist)
1805 (s, C = O stretch)	976 (w, H – C – H twist)
1644 (w, H – C – H bend)	918 (w, C – C stretch)
1641 (w, H – C – H bend)	898 (w, C – C stretch)
1631 (w, H – C – H bend)	874 (w, C – N stretch)
1622 (w, H – C – H bend)	857 (w, C – N stretch)
1502 (w, C – C stretch)	821 (w, H – C – H twist)
1486 (w, C – N stretch)	716 (w, C – O stretch)
1415 (w, C – N stretch)	684 (w, C – C, C – O stretches)
1397 (w, H – C – H twist)	677 (w, C – O stretch)
1338 (w, H – C bend)	633 (w)
1290 (m, C – O stretch)	572 (w)
1266 (m, H – C – H twist)	561 (w)
1256 (s, C – O stretch)	542 (w)
1252 (m, C – O stretch)	516 (w)
1242 (w, C – O stretch)	486 (w)
1199 (w, V = O stretch)	459 (w)
1166 (w, C – N – C bend)	436 (w)

actual spectrum. DFT assigned the peak at 1812 cm^{-1} as a carbonyl stretch, and so the peak at 1641 cm^{-1} in the actual spectrum is most likely a carbonyl stretch. A strong broad peak centered at 3437 cm^{-1} appears in the actual infrared spectrum, and this peak comprises the νO-H stretches of the associated water molecules. No water molecules were included in the DFT calculation, and so this broad peak did not appear in the calculated spectrum. The calculated $\nu_{V=O}$ stretching frequency is 1199 cm^{-1}, which is

higher than the range of *ca.* 875 to 1035 cm^{-1}, where $\nu_{V=O}$ stretching frequencies are commonly observed [27]. Four peaks from 932 to 968 cm^{-1} are observed in the actual infrared spectrum, and any of these may represent $\nu_{V=O}$ stretching. However, a visual comparison of the two spectra matches the calculated peak at 1199 cm^{-1} with the experimental peak at 1088 cm^{-1}, which implies that this peak at 1088 cm^{-1} is a $\nu_{V=O}$ stretching frequency. The vibrational modes below 677 cm^{-1} appeared to be complicated, and so no effort to label the assignments for these vibrations was made.

2.5 Electronic Absorption Data

The electronic absorption spectrum of an aqueous solution of $Na_2[(VO)_2(ttha)] \cdot 8 H_2O$ with a range of wavelengths from 400 to 900 nm is shown in Figure 2.6, and with a range of wavelengths from 200 to 400 nm in Figure 2.7. For the sake of comparison, the TDDFT calculated spectra are included in Figures 2.6 and 2.7 as well. The experimental spectrum in Figure 2.6 features two broad peaks centered at 586 nm (ε = 33 L mol^{-1} cm^{-1}) and 770 nm (ε = 38 L mol^{-1} cm^{-1}), and these absorption peaks have been reported previously [28]. The TDDFT calculated spectrum features two similar absorptions at 656 and 798 nm, and these peaks are assigned as HOMO→LUMO+2 and HOMO→LUMO transitions, respectively, in the α spin set of molecular orbitals. Two d orbitals, one on each vanadium atom, feature prominently in the α HOMO, the α LUMO, and the α LUMO+2 orbitals, which are shown in Figure 2.8. Hence, these transitions are characterized by small molar absorptivity constants because they are primarily d→d transitions.

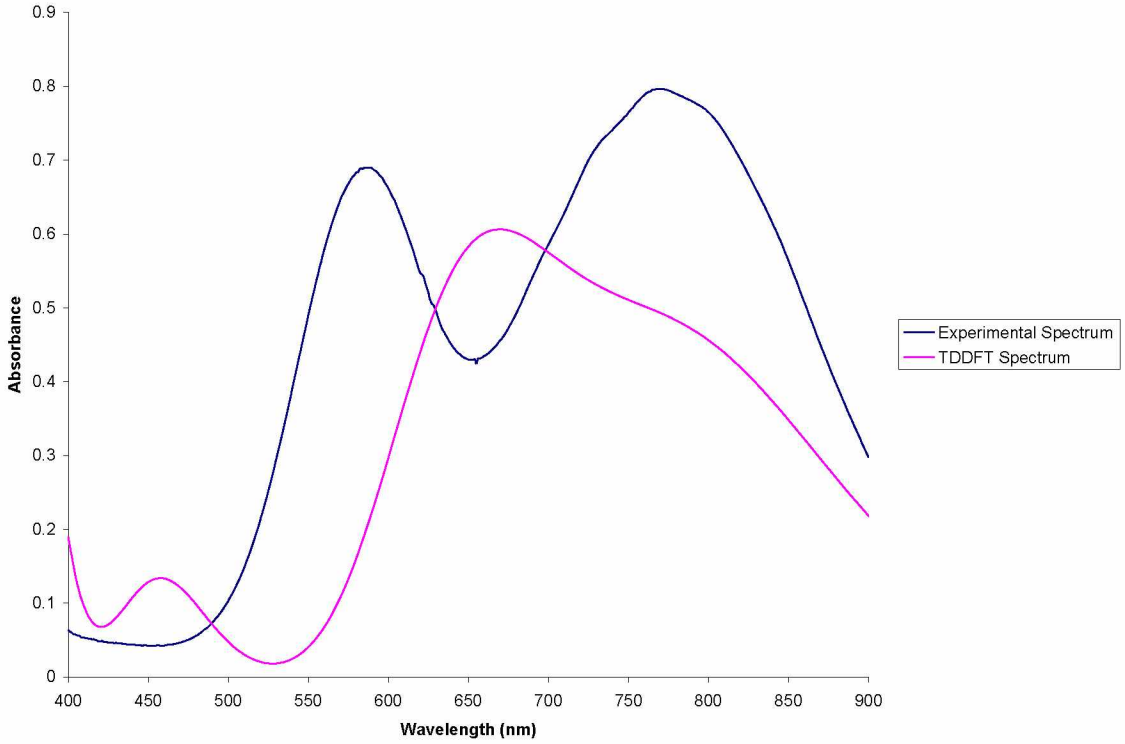

Figure 2.6. Electronic Absorption Spectrum from 400 to 900 nm of an Aqueous Solution of $Na_2[(VO)_2(ttha)] \cdot 8\ H_2O$, and the Time-Dependent Density Functional Theory Calculated Absorption Spectrum of $[(VO)_2(ttha)]^{2-}$.

In addition, a small broad peak centered at 458 nm appears in the TDDFT spectrum, but this peak is not obvious in the experimental spectrum. TDDFT assigned this peak as the α spin HOMO-1→LUMO+5 transition. The TDDFT calculated transitions, their peak assignments, and their oscillator strengths are summarized in Table 2.3. Moreover, the experimental peaks and their molar absorptivity constants are listed in Table 2.3 as well, for comparison.

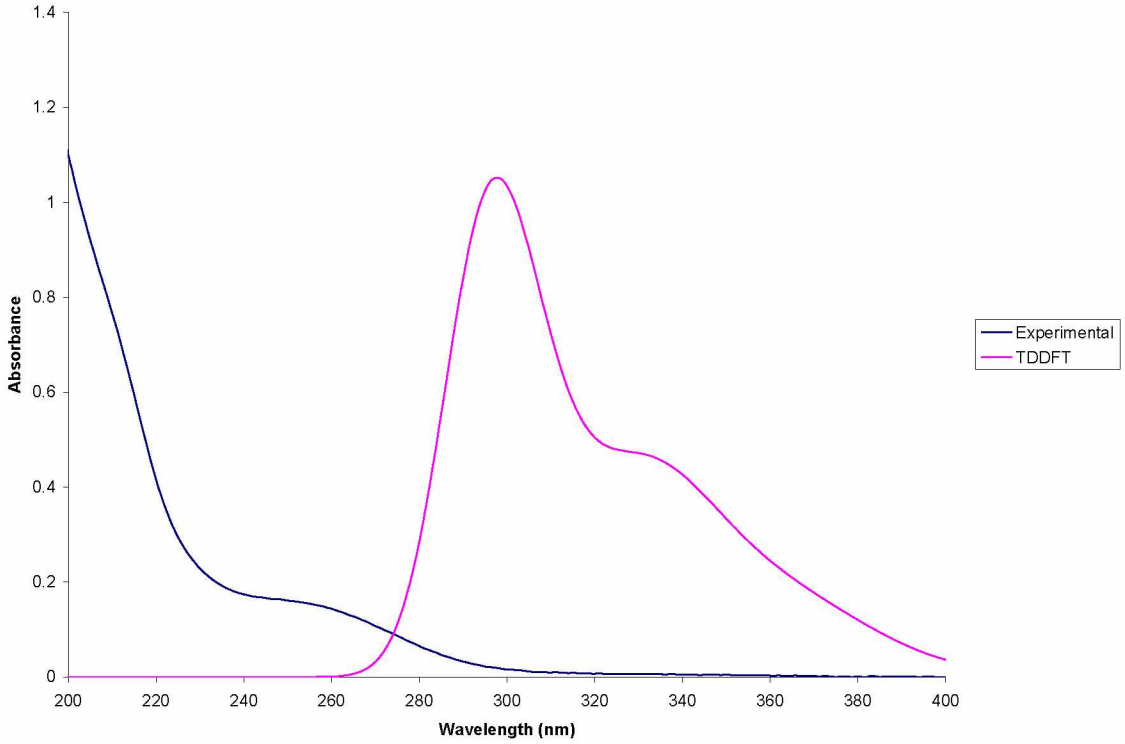

Figure 2.7. Electronic Absorption Spectrum from 200 to 400 nm of an Aqueous Solution of $Na_2[(VO)_2(ttha)] \cdot 8\ H_2O$, and the Time-Dependent Density Functional Theory Calculated Absorption Spectrum of $[(VO)_2(ttha)]^{2-}$.

The experimental and calculated spectra over the wavelength range of 200 to 400 nm (Figure 2.7) have similar shapes. The experimental spectrum features a small broad peak centered near 255 nm and a taller broad peak that is centered near 200 nm. (As shown in Figure 2.7, this taller peak is not fully represented because the lower spectral limit is 200 nm). The TDDFT spectrum also features a small broad peak centered near 330 nm and a taller broad peak centered near 297 nm. Both peaks are composites of several transitions, as shown in Table 2.3.

Table 2.3. Comparison of Observed Electronic Transitions with TDDFT Calculated Transitions in Both the α-Spin and the β-Spin Molecular Orbitals.

α-Spin	**β-Spin**	**Osc. Strength**	**Calc. λ (nm)**	**Obs. λ (nm), ε (L mol^{-1} cm^{-1})**	
H→L		0.0019	798.1	770	38
H-1→L		0.0002	796.4		
H→L+2		0.0025	656.4	586	33
H-1→L+2		0.0004	655.7		
H-1→L+5		0.0007	457.8		
H→L+5			457.6		
H→L+1			371.4		
H-1→L+1		0.0029	371.1		
H-1→L+2		0.0007	352.2		
H-1→L+3		0.0010	352.1		
H→L+7			343.1		
H-1→L+7		0.0004	343.1		
H→L+4		0.0033	341.0		
H-1→L+4			340.3		
	H→L	0.0007	337.9		
	H-1→L		337.7		
H-1→L+11		0.0032	330.0	255	3480
H→L+11		0.0003	330.0		
	H-3→L+1	00010	328.5		
	H-2→L+1	0.0007	328.5		
H-9→L+3		0.0019	324.9		
H-8→L+2		0.0007	324.9		
H-11→L		0.0011	310.7		
H-8→L		0.0004	310.6		
H-7→L+2		0.0002	310.5		
H-7→L+2		0.0001	310.4		
H-2→L		0.0057	297.8	*ca.* 200	> 13900
H-3→L		0.0016	297.8		
	H-4→L	0.0172	296.5		
	H-5→L	0.0032	296.5		

α HOMO

α LUMO

α LUMO+2

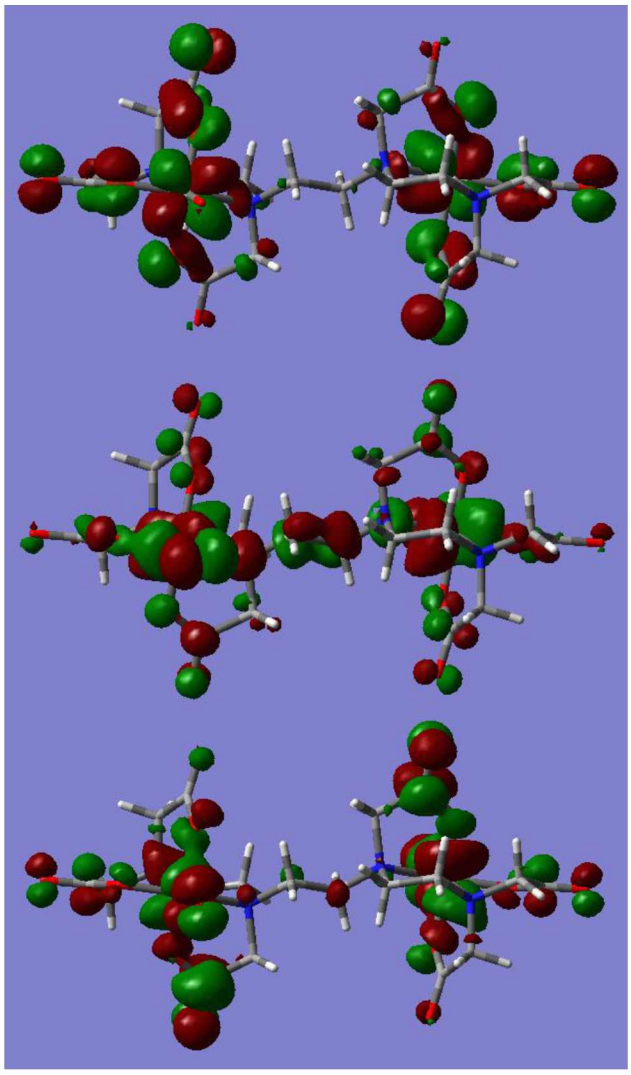

Figure 2.8. Three Molecular Orbitals of $[(VO)_2(ttha)]^{2-}$ (the HOMO, the LUMO, and the LUMO+2) From the α Spin Set of the TDDFT Calculations.

2.6 Electron Spin Resonance Data

As shown in Figure 2.8, DFT predicts the HOMO to consist partly of two d orbitals, one on each vanadium center. The HOMO-1 orbital (not shown) also consists partly of two d orbitals, one on each vanadium center. Hence, the two unpaired electrons

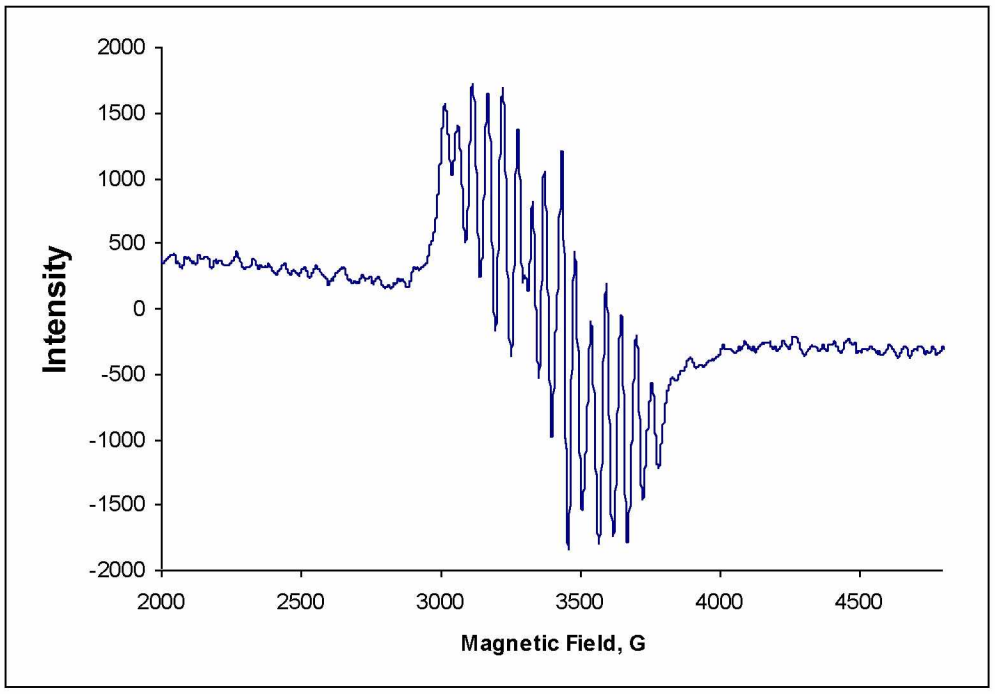

Figure 2.9. Electron Spin Resonance Spectrum of $Na_2[(VO)_2(ttha)] \cdot 8\ H_2O$ in Aqueous Solution at Room Temperature.

in $[(VO)_2(ttha)]^{2-}$ exist simultaneously at both vanadium centers. In order to test this prediction, the first derivative electron spin resonance spectrum (shown in Figure 2.9) of an aqueous solution of $Na_2[(VO)_2(ttha)] \cdot 8\ H_2O$ at room temperature was obtained. Fifteen peaks are observed, which is consistent with the notion that the two odd electrons are in vanadium-based molecular orbitals since ^{51}V is 100% abundant and the nuclear spin is 7/2. For the spectrum shown in Figure 2.9, g = 1.96, and the hyperfine splitting constant (a) is 56 gauss. The electron spin resonance spectrum of $Na_2[(VO)_2(ttha)] \cdot 8\ H_2O$ resembles those of some dinuclear vanadyl(IV) tartrate [29] and dinuclear vanadyl(IV) citrate complexes [30].

2.7 pH and Thermal Stability of $Na_2[(VO)_2(ttha)] \cdot 8\ H_2O$

$Na_2[(VO)_2(ttha)] \cdot 8\ H_2O$ is very stable chemically in aqueous solution at neutral pH. In order to characterize the stability of this complex in solution as the pH is varied, five ultraviolet-visible absorption spectra of aqueous solutions of $Na_2[(VO)_2(ttha)] \cdot 8\ H_2O$ at the pH values of 0.80, 1.05, 6.91, 10.96, and 11.95 were recorded, and these spectra are superimposed on the same plot in Figure 2.10. The characteristic two

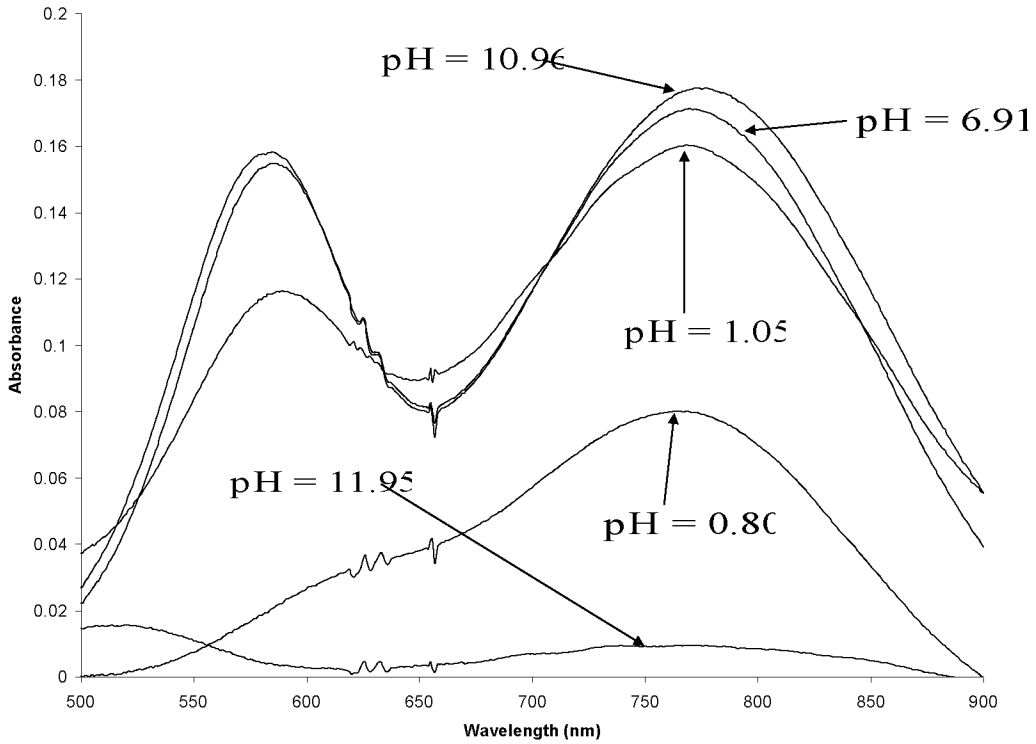

Figure 2.10. Visible Absorption Spectra of Aqueous Solutions of $Na_2[(VO)_2(ttha)] \cdot 8\ H_2O$ at Different pH Levels.

absorption peaks at 586 and 770 nm are clearly observed in the solutions with pH values between 1.05 and 10.96, indicating that the complex is stable in solution in this pH range. At a pH of 11.95, no $[(VO)_2(ttha)]^{2-}$ is observed in the electronic absorption spectrum,

which is consistent with an earlier report concerning the stability of this ion in solution with a pH > 10 [28]. Likewise, at the acidic pH of 0.80, no $[(VO)_2(ttha)]^{2-}$ is observed. In the very acidic solution with a pH of 0.80, the primary absorption peaks observed at 630 and 770 nm represent the hydrated vanadyl cation, $[(H_2O)_5VO]^{2+}$ [31].

Additionally the thermal stability of both the solid state and aqueous solution was investigated. The solution and powder were both heated to 100 ºC for approximately one day. The after heating $Na_2[(VO)_2(ttha)] \cdot 8\ H_2O$ powder for the allotted time the powder was dissolved in water stored at room temperature before analysis. Both solid state and aqueous solutions appear to remain intact as indicated in Figure 2.11.

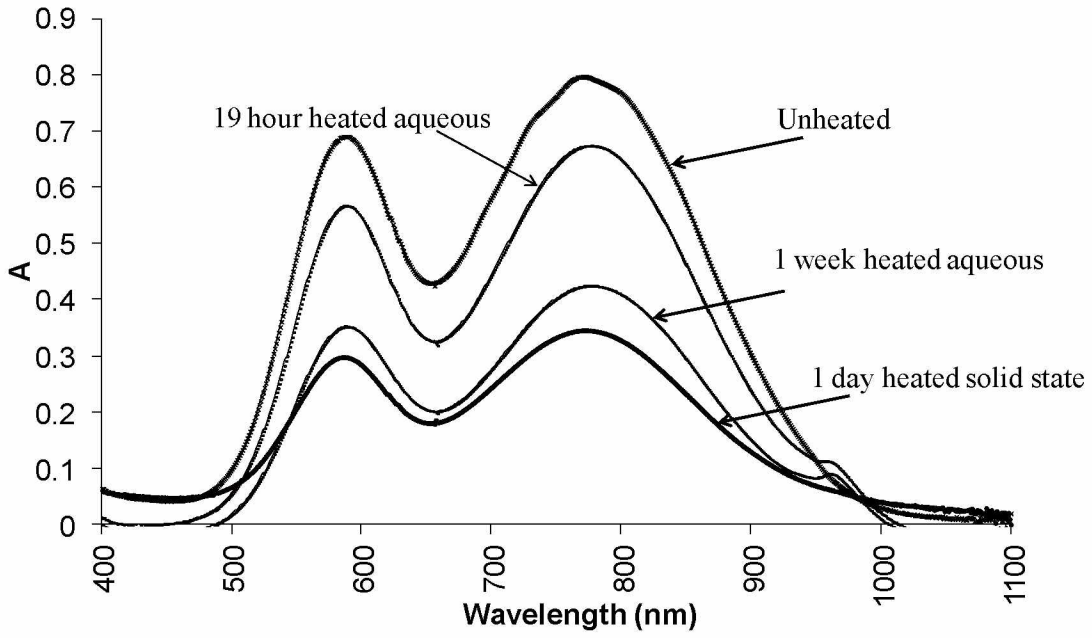

Figure 2.11. Visible Absorption Spectra of Aqueous Solutions of $Na_2[(VO)_2(ttha)] \cdot 8$ Thermal Stability Studies.

There is however a small peak centered at 955 nm that begins to form in the aqueous solution after one hour of heating, and may provide evidence of a slight decomposition.

2.8 Experimental Details

All reactions were carried out open to air, using deionized water as the solvent. Infrared spectra were recorded as KBr pellets on a Nicolet Magna−IR 560 spectrometer, and the data are reported in cm^{-1}. Electron spin resonance spectra of aqueous solutions of $Na_2[(VO)_2(ttha)] \cdot 8\ H_2O$ at room temperature were recorded using a Bruker EMX spectrometer. UV-vis absorption data were obtained using a Hewlett-Packard Model 8453 spectrometer in aqueous solution. Elemental analyses were carried out by Atlantic Microlab, Inc. (Norcross, GA). Triethylenetetraamine-N, N, N', N", N'", N'"-hexaacetic acid was purchased from Aldrich and used as received. Vanadyl(IV) acetate was prepared according to a published procedure [32].

2.8.1 Synthesis of $[VO(H_2O)_5][(VO)_2(ttha)] \cdot 4\ H_2O$

A mixture of H_6ttha (0.352 g, 0.712 mmol) and $OV(OOCCH_3)_2$ (0.396 g, 2.14 mmol) in deionized water (25 mL) was stirred at 55°C for two hours. The blue homogeneous solution was cooled to room temperature and set aside for one week. Blue crystals precipitated and were isolated and air-dried, yield = 0.386 g (63.7%). This compound was characterized by single crystal X-ray diffraction; the structural data were identical to the data already published for this compound [1] and are not reported.

2.8.2 Synthesis of $Na_2[(VO)_2(ttha)] \cdot 8\ H_2O$

An aqueous solution (10 mL) of H_6ttha (0.061 g, 0.12 mmol) was titrated with a 0.118 M NaOH solution (6.3 mL, 0.74 mmol) to deprotonate the acidic protons on the H_6ttha molecule. The mixture was stirred for 30 minutes at room temperature after completing the titration. Solid $[VO(H_2O)_5][(VO)_2(ttha)] \cdot 4\ H_2O$ (0.211 g, 0.248 mmol) was added, and the mixture was stirred at 60°C for one hour. The blue homogeneous solution was cooled to room temperature and set aside for one week. Blue crystals precipitated and were isolated and air-dried, yield = 0.197 g (67.4%). Although X-ray diffraction revealed this product to be an octahydrate, the elemental analysis results were more consistent with a pentahydrate. For the octahydrate, anal. calc. for $C_{18}H_{40}N_4Na_2O_{22}V_2$: C, 26.61%; H, 4.96%; N, 6.90%. For the pentahydrate, anal. calc. for $C_{18}H_{34}N_4Na_2O_{19}V_2$: C, 28.51%; H, 4.52%; N, 7.39%. Found: C, 28.57%; H, 4.41%; N, 7.33%. IR data: 3437 (s, broad), 2979 (w), 2945 (w), 1641 (vs), 1471 (w), 1464 (w), 1429 (w), 1382 (s), 1361 (s), 1324 (m), 1315 (m), 1289 (w), 1274 (w), 1125 (w), 1088 (m), 1058 (w), 1014 (w), 968 (s), 953 (m), 942 (m), 932 (m), 873 (m), 820 (w), 784 (w), 746 (w), 725 (w), 650 (w), 595 (w), 549 (w), 481 (m), 440 (m), 424 (m).

2.8.3 Hydration Determination

A sample of $Na_2[(VO)_2(ttha)] \cdot 8\ H_2O$ (53.5 mg) was stored at 60°C under a pressure of 2.5 Torr for 14.5 hours. No change in the appearance of the sample was observed, and the mass of the sample was found to be 43.4 mg (6.49×10^{-5} mol) after the

14.5 hour period. The mass of water evolved from the sample is 10.1 mg (5.61×10^{-4} mol), which corresponds to 8.64 water molecules per $[(VO)_2(ttha)]^{2-}$ anion.

2.8.4 X-Ray Diffraction Studies

Royal blue crystals of $Na_2[(VO)_2(ttha)] \cdot 8\ H_2O$ were obtained from aqueous solution at room temperature. X-ray diffraction data were collected on a Bruker P4 diffractometer equipped with a SMART CCD detector. Crystal data and data collection and refinement parameters are summarized in Table 2. The structure, solved by using direct methods and standard difference map techniques, was refined by full-matrix least-squares of F^2 with SHELXTL (Version 6.10) [33]. Hydrogen atoms were included in calculated positions.

2.8.5 Density Functional Theory (DFT) Calculations

The structure of $[(VO)_2(ttha)]^{2-}$ was optimized for the triplet state using the DFT method in the GAUSSIAN 03 program [34], with the LANL2MB basis set [35] and B3LYP functional [36, 37] in the gas phase. The ultraviolet-visible absorption spectrum was calculated with the time-dependent density functional theory method [38] of the spin-allowed state of the triplet-triplet transition. Vibrational calculations were completed without solvent interactions, and no negative frequencies were found in the calculated infrared spectrum. Calculated spectra were post-processed using SWizard software [39].

2.9 Conclusion

The goal of this research was to propose a transferrin model which incorporated the dual vanadium binding sites, octahedral geometry, and the ability for transferrin to bind to vanadium in the oxidation state of V^{IV}. The proposed complex, $[(VO)_2(ttha)]Na_2 \cdot 8H_2O$, satisfies these constraints. The EPR and X-ray crystal data confirm that the ttha ligand coordinated to two vanadium atoms with the oxidation state of V^{IV}. X-ray crystal data confirmed that the vanadium centers have octahedral geometry. Additionally, $[(VO)_2(ttha)]Na_2 \cdot 8H_2O$, like transferrin, coordinates to the vanadium centers by oxo-vanadium and nitrogen-vanadium bonds.

Though this model meets the conditions desired for a realistic vanadium-transferrin model, the model is still not perfect. Transferrin is expected to bind to vanadium through one histidine, one aspartate, and two tyrosine residues, and an auxillary carbonate anion. The model does not incorporate the coordination of the vanadium center using amino acids or the use of an auxiliary ligand.

2.10 Supplementary Data

CCDC 724901 contains the supplementary crystallographic data for $Na_2[(VO)_2(ttha)] \cdot 8 H_2O$. These data can be obtained free of charge via http://www.ccdc.cam.ac.uk/conts/retrieving.html, or from the Cambridge Crystallographic Data Centre, 12 Union Road, Cambridge CB2 1EZ, UK; fax: (+44) 1223-336-033; or email: deposit@ccdc.cam.ac.uk.

2.11 References

1. W. Shi, X.-Y. Chen, B. Zhao, A. Yu, H.-B. Song, P. Cheng, H.-G. Wang, D.-Z. Liao, S.-P. Yan, Inorg. Chem. 45 (2006) 3949.
2. J. Ya-Qi, X. Zhao-Xiong, Chinese J. Struct. Chem. 22 (2003) 423.
3. L.-S. Long, Y.-P. Ren, R.-B. Huang, L.-S. Zheng, S. W. Ng, Acta Cryst. E59 (2003) m456.
4. G. D. Fallon, B. M. Gatehouse, Acta Cryst. B32 (1976) 71.
5. A. Neves, S. M. de Moraes Romanowski, A. J. Bortoluzzi, A. S. Mangrich, Inorg. Chim. Acta 313 (2001) 137.
6. A. Neves, A. S. Ceccatto, C. Erasmus-Buhr, S. Gehring, W. Haase, H. Paulus, O. R. Nascimento, A. A. Batista, Chem. Commun. 1993, 1782.
7. T. W. Hambley, R. J. Judd, P. A. Lay, Inorg. Chem. 31 (1992) 343.
8. T. Kiss, T. Jakusch, S. Bouhsina, H. Sakurai, E. A. Enyedy, Eur. J. Inorg. Chem. (2006) 3607.
9. A. Gorzsás, I. Andersson, L. Pettersson, Eur. J. Inorg. Chem. 2006, 3559.
10. D. C. Crans, J. J. Smee, E. Gaidamauskas, L. Yang, Chem. Rev. 104 (2004) 849.
11. M. H. Nagaoka, T. Yamazaki, T. Maitani, Biochem. Biophys. Res. Commun. 296 (2002) 1207.
12. T. Kiss, E. Kiss, E. Garribba, H. Sakurai, J. Inorg. Biochem. 80 (2000) 65.
13. J. A. Saponja, H. J. Vogel, J. Inorg. Biochem. 62 (1996) 253.
14. N. D. Chasteen, Met. Ions Biol. Syst. 31 (1995) 231.
15. N. D. Chasteen, J. K. Grady, C. E. Holloway, Inorg. Chem. 25 (1986) 2754.

16. W. R. Harris, C. J. Carrano, J. Inorg. Biochem. 22 (1984) 201.

17. A. Neves, A.S. Ceccatto, C. Erasmus-Buhr, S. Gehring, H. Paulus, O.R. Nascimento, A.A. Bastista, Chem. Commun. (1993) 1782-84.

18. T.W. Hambley, R.J Judd, Inorg. Chem. 31 (1992) 343-45.

19. W. A. Nugent, J. M. Mayer, Metal – Ligand Multiple Bonds, Wiley & Sons, 1988.

20. D. C. Crans, A. D. Keramidas, M. Mahroof-Tahir, O. P. Anderson, M. M. Miller, Inorg. Chem. 35 (1996) 3599.

21. G. I. Filin, V. N. Markin, Bull. Leningrad Univ., Phys. Chem. (1977) 141.p

22. Z. Kangjing, L. Xiaopin, Chin. J. Struct. Chem. 6 (1987) 14.

23. W. R. Scheidt, R. Countryman, J. L. Hoard, J. Am. Chem. Soc. 93 (1971) 3878.

24. W. R. Scheidt, D. M. Collins, J. L. Hoard, J. Am. Chem. Soc. 93 (1971) 3873.

25. M. Shimoi, Y. Saito, H. Ogino, Chem. Lett. (1989) 1675.

26. J. C. Pessoa, M. J. Calhorda, I. Cavaco, I. Correia, M. T. Duarte, V. Felix, R. T. Henriques, M. F. M. Piedade, I. Tomaz, Dalton Trans. (2002) 4407.

27. J. Selbin, L. H. Holmes Jr., S. P. McGlynn, J. Inorg. Nucl. Chem. 25 (1963) 1359.

28. A. Napoli, Gazz. Chim. Ital. 106 (1976) 597.

29. H. Sakurai, S. Funakoshi, Y. Adachi, Pure Appl. Chem. 77 (2005) 1629.

30. M. Velayutham, B. Varghese, S. Subramanian, Inorg. Chem. 37 (1998) 1336.

31. C. E. Ophardt, S. Stupgia, J. Chem. Educ. 61 (1984) 1102.

32. R. C. Paul, S. Bhatia, A. Kumar, Inorg. Synth. 13 (1971) 181.

33. G. M. Sheldrick. SHELXTL, An Integrated System for Solving, Refining, and Displaying Crystal Structures from Diffraction Data; University of Göttingen, Göttingen, Federal Republic of Germany, 1981.

34. M. J. Frisch, G. W. Trucks, H. B. Schlegel, G. E. Scuseria, M. A. Robb, J. R. Cheeseman, J. A. Montgomery Jr., T. Vreven, K. N. Kudin, J. C. Burant, J. M. Millam, S. S. Iyengar, J. Tomasi, V. Barone, B. Mennucci, M. Cossi, G. Scalmani, N. Rega, G. A. Petersson, H. Nakatsuji, M. Hada, M. Ehara, K. Toyota, R. Fukuda, J. Hasegawa, M. Ishida, T. Nakajima, Y. Honda, O. Kitao, H. Nakai, M. Klene, X. Li, J. E. Knox, H. P. Hratchian, J. B. Cross, C. Adamo, J. Jaramillo, R. Gomperts, R. E. Stratmann, O. Vazyev, A. J. Austin, R. Cammi, C. Pomelli, J. W. Ochterski, P. Y. Ayala, K. Morokuma, G. A. Voth, P. Salvador, J. J. Dannenberg, V. G. Zakrzewski, S. Dapprich, A. D. Daniels, M. C. Strain, O. Farkas, D. K. Malick, A. D. Rabuck, K. Raghavachari, J. B. Foresman, J. V. Ortiz, Q. Cui, A. G. Baboul, S. Clifford, J. Cioslowski, B. B. Stefanov, G. Liu, A. Liashenko, P. Piskorz, I. Komaromi, R. L. Martin, D. J. Fox, T. Keith, M. A. Al-Laham, C. Y. Peng, A. Nanayakkara, M. Challacombe, P. M. W. Gill, B. Johnson, W. Chen, M. W. Wong, C. Gonzalez, J. A. Pople, GAUSSIAN 03, Revision B.03, Gaussian, Inc., Pittsburgh, PA, 2003.

35. P. J. Hay, W. R. Wadt, J. Chem. Phys. 82 (1985) 299.

36. A. D. Becke, J. Chem. Phys. 98 (1993) 5648.

37. C. Lee, W. Yang, R. G. Parr, Phys. Rev. B 37 (1988) 785.

38. M. E. Casida, in: J. M. Seminario (Ed.), Recent Developments and Applications in Modern Density Functional Theory, Theoretical and Computational Chemistry, vol. 4, Elsevier, Amsterdam, 1996.

39. S. I. Gorelsky, SWizard Program, http://www.sg-chem.net/, 2008.

Chapter 3 Coordination of 4-Subsituted-2,6-Pyridinedimethanol Ligands to Vanadate[1]

3.1 Introduction

A variety of three-coordinate O,N,O' ancillary ligands have recently been complexed to vanadate centers, and a number of these complexes have been structurally characterized by single crystal X-ray diffraction [1 – 13]. Some of these compounds, such as $[VO_2(dipic)]^-$ and $[VO_2(dipic\text{-}OH)]^-$, have been shown to be effective drugs for treating hyperglycemia in diabetic rats [14 – 17]. 2,6-Pyridinedimethanolate is structurally similar to, but chemically distinct from, 2,6-pyridinedicarboxylate, and the first vanadate complex stabilized by the pyridinedimethanolate ligand, namely $Na[VO_2(pydim)] \cdot 4\ H_2O$, was reported by the Howard Group in 2006 [18]. 2,6-pyridinedimethanolate binds to the vanadium center using a alcohol functional group whereas 2,6-pyridinedicarboxylate binds to the vanadium center with a carboxylic acid functional group. Little is known concerning how effective these O,N,O' ancillary ligands like dipic and pydim are for stabilizing dioxovanadium compounds however. For instance, are electron-donating ancillary ligands better than electron-withdrawing ligands for stabilizing dioxovanadium compounds? Is $[VO_2(pydim)]^-$ more stable than $[VO_2(dipic)]^-$? The aim of this present work is to address these questions.

---

[1] Z.N. Pickett, W.A. Howard, C.R. Graves, J Chem Crystallogr. 38 (2008) 717.

3.2 Results

The two novel compounds, $Na[VO_2(pydim\text{-}Cl)] \cdot 2\ H_2O$ and $Na[VO_2(pydim\text{-}NMe_2)] \cdot 3\ H_2O$ were prepared as shown in Figure 3.1, similar to the preparation of $Na[VO_2(pydim)] \cdot 4\ H_2O$ [18].

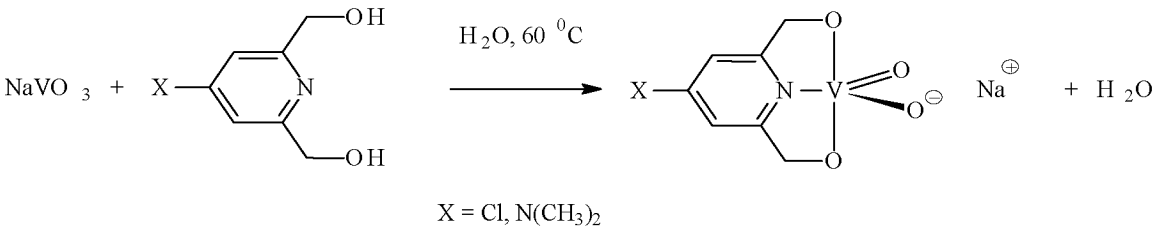

Figure 3.1. Syntheses of $Na[VO_2(pydim\text{-}Cl)] \cdot 2\ H_2O$ and $Na[VO_2(pydim\text{-}NMe_2)] \cdot 3\ H_2O$.

Although neither $Na[VO_2(pydim\text{-}Cl)] \cdot 2\ H_2O$ nor $Na[VO_2(pydim\text{-}NMe_2)] \cdot 3\ H_2O$ were structurally characterized by single crystal X-ray diffraction, due to the inability to grow suitable crystals, these compounds were characterized by NMR spectroscopy, infrared spectroscopy, and elemental analysis. Thus, $Na[VO_2(pydim\text{-}Cl)] \cdot 2\ H_2O$ is characterized by two resonances in the ^1H NMR spectrum (D_2O); a methylene peak at δ 5.42 ppm (s, 4 H), and a peak in the aromatic region at δ 7.45 ppm (s, 2 H). The ^{51}V NMR spectrum consists of one singlet at -516 ppm. For the sake of comparison, the ^{51}V NMR spectra (D_2O) of $Na[VO_2(dipic)]$ and $Na[VO_2(pydim)] \cdot 4\ H_2O$ feature singlets at -533 and -508 ppm, respectively [15, 18]. Moreover, stretching frequencies

for terminal V=O moieties typically range between *ca.* 875 and 1035 cm^{-1} [19], and the infrared spectrum of $Na[VO_2(pydim\text{-}Cl)] \cdot 2\ H_2O$ features a strong peak at 916 cm^{-1}; no effort to prove the terminal $\nu_{V=O}$ stretching frequency was made however. $Na[VO_2(pydim\text{-}NMe_2)] \cdot 3\ H_2O$ is characterized by ^1H NMR resonances (D_2O) at δ 2.95 ppm (dimethylamino hydrogens), 5.28 ppm (methylene hydrogens), and 6.40 ppm (aromatic ring hydrogens), and by a singlet at δ -506 ppm in the ^{51}V NMR spectrum. Furthermore, a very strong absorbance at 914 cm^{-1} appears in the infrared spectrum, consistent with a terminal $\nu_{V=O}$ stretch.

In order to assess the stability of the various vanadium complexes $[VO_2(pydim\text{-}X)]^-$ (X = H, Cl, NMe_2) and $[VO_2(dipic)]^-$, with a competing ligand, each of these complexes were treated with H_2pydim-X or H_2dipic and the mixtures were monitored by ^1H NMR spectroscopy. The results are summarized in Figure 3.2. Thus, 2,6-pyridinedimethanol easily displaces 4-chloro-2,6-pyridinedimethanol from $[VO_2(pydim\text{-}Cl)]^-$ in aqueous solution at room temperature, affording $[VO_2(pydim)]^-$ and H_2pydim-Cl. 4-dimethylamino-2,6-pyridinedimethanol reacts with $[VO_2(pydim)]^-$, yielding $[VO_2(pydim\text{-}NMe_2)]^-$ and free 2,6-pyridinedimethanol. Finally, 2,6-dipicolinic acid replaces the 4-dimethylamino-2,6-pyridinedimethanolate ligand in $[VO_2(pydim\text{-}NMe_2)]^-$, producing $[VO_2(dipic)]^-$ and H_2pydim-NMe_2. All of the reactions shown in Figure 3.2 are reversible, but the arrows are drawn in the thermodynamically favored direction, as judged by ^1H NMR spectroscopy.

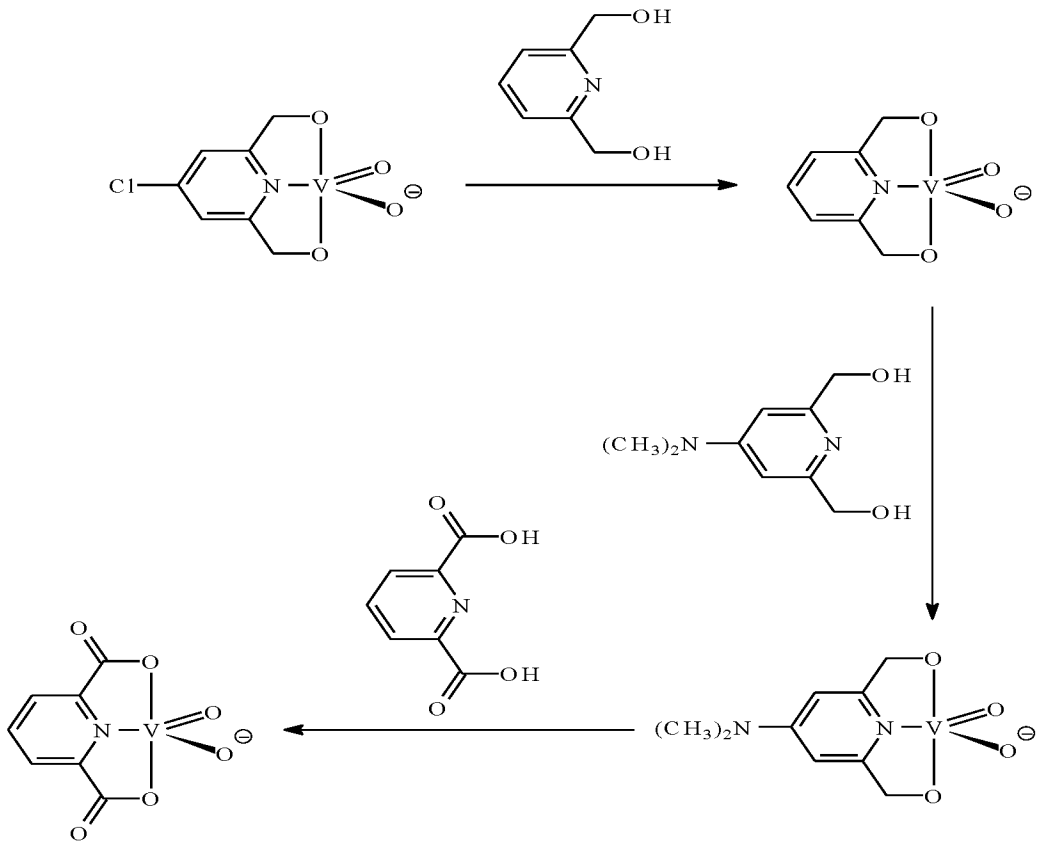

Figure 3.2. Summary of Ligand Displacement Reactions Involving $[VO_2(pydim\text{-}X)]^-$ (X = H, Cl, NMe_2) and $[VO_2(dipic)]^-$.

Thus, in the series of $[VO_2(pydim\text{-}X)]^-$ ions, the relative stabilities are: $[VO_2(pydim\text{-}NMe_2)]^- > [VO_2(pydim)]^- > [VO_2(pydim\text{-}Cl)]^-$, with $[VO_2(pydim\text{-}NMe_2)]^-$ as the most stable and $[VO_2(pydim\text{-}Cl)]^-$ as the least stable. These three complex ions and $[VO_2(dipic)]^-$ were modeled by DFT calculations, which revealed the charges at the vanadium centers. The DFT calculated charges are as follows: $[VO_2(pydim\text{-}NMe_2)]^-$, -0.340; $[VO_2(pydim)]^-$, -0.303; and $[VO_2(pydim\text{-}Cl)]^-$, -0.291. Hence, there exists more electron density on vanadium in $[VO_2(pydim\text{-}NMe_2)]^-$ than in either $[VO_2(pydim)]^-$ or $[VO_2(pydim\text{-}Cl)]^-$, and so the pydim-$NMe_2$ ligand is a stronger electron donor than either

the pydim or the pydim-Cl ligand. Likewise, the pydim ligand is a stronger electron donor than is the pydim-Cl ligand. In the series of pydim-X complexes, the better the pydim-X ligand is as an electron donor, the more stable the vanadium complex is. The DFT calculated atomic coordinates and total energy for the $[VO_2(pydim\text{-}X)]^-$ ions can be found in Tables A5 thru A7 of the Appendix. DFT calculated atomic coordinates and total energy for the $[VO_2(dipic)]^-$ ion can be found in Table A8 of the Appendix

$[VO_2(dipic)]^-$ was also modeled by DFT calculations, and the calculated charge on the vanadium center was -0.167. Thus, the dipicolinate ligand is, according to the DFT calculation, the weakest electron donor in this study. Yet when dipic was introduced as a competing ligand $[VO_2(dipic)]^-$ was the predominant vanadium species observed by NMR. Though the dipic ligand, according to DFT calculations, is a weaker electron donor, other factors contribute to its ability to compete for the available vanadium. The carboxylic acid functional groups on dipic makes dipic a stronger acid than the alcohol functional groups on pydim. The ligands ability to deprotonate the oxygen atoms in the binding site must be an influential factor in the ligands ability to take up vanadium.

3.3 Protonated Pyridinedimethanol Ligands

When the pH of an aqueous solution of either $Na[VO_2(pydim\text{-}Cl)] \cdot 2\ H_2O$ or $Na[VO_2(pydim\text{-}NMe_2)] \cdot 3\ H_2O$ is lowered by the addition of HCl (aq), the complex decomposes, and the protonated ancillary ligand, either $(H_3pydim\text{-}Cl)^+Cl^-$ or $(H_3pydim\text{-}NMe_2)^+Cl^-$, is formed. Alternatively, these protonated ligands can be made simply by the addition of HCl (aq) to aqueous solutions of $H_2pydim\text{-}Cl$ or $H_2pydim\text{-}NMe_2$. The

compounds $(H_3pydim\text{-}Cl)^+Cl^-$ and $[(H_3pydim\text{-}NMe_2)^+Cl^-]_2(H_2O)$ were crystallized from aqueous solutions and structurally characterized by single crystal X-ray diffraction [20].

The crystal, intensity collection, and refinement data for the X-ray structures of $H_3(pydim\text{-}Cl)Cl$ and $[H_3(pydim\text{-}NMe_2)Cl]_2(H_2O)$ are summarized in Table A2 in the Appendix, while selected metrical data for both structures are reported in Table 3.1. Thermal ellipsoid plots for both structures are shown in Figures 2.3 and 2.4.

For the sake of comparison, it should be noted that the X-ray structures of two related compounds, namely 4-dimethylaminopyridinium chloride dihydrate and anhydrous 4-dimethylaminopyridinium chloride, were published in 1977 [21] and in 1992 [22], respectively. Moreover, the X-ray structure of a cyclophane derivative with a 4-dimethylamino-2,6-pyridinedimethanolato moiety [23] and the X-ray structure of 4-chloropyridinium chloride [24] have also been reported recently.

In the case of 4-dimethylaminopyridinium chloride dihydrate, it was found that there were two sets of two independent 4-dimethylaminopyridinium cations ($Z = 4$) with different bond lengths and bond angles in the unit cell. In contrast, there was only one type of cation in the unit cell of anhydrous 4-dimethylaminopyridinium chloride. In the present case involving 4-dimethylamino-2,6-*bis*(hydroxymethyl)pyridinium chloride, the eight cations in the unit cell are structurally indistinguishable. The pyridine rings in both

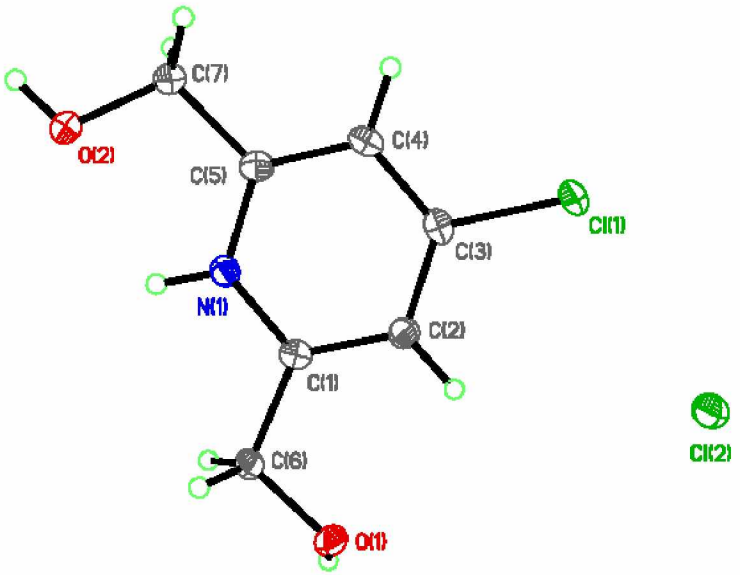

Figure 3.3. Thermal Ellipsoid Plot of 4-chloro-2,6-*bis*(hydroxymethyl)pyridinium chloride.

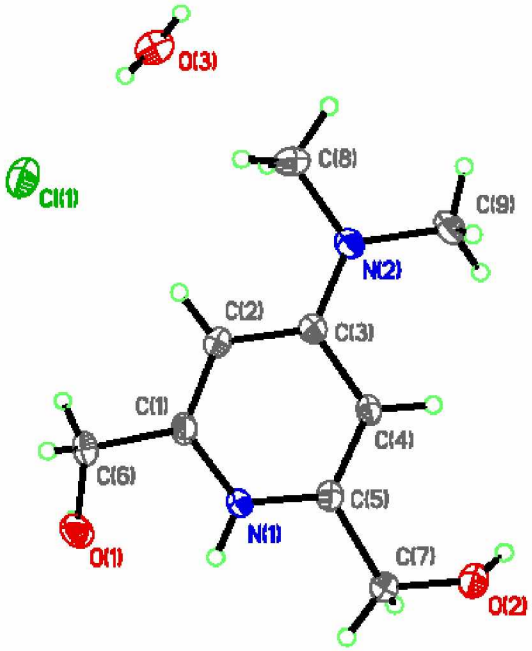

Figure 3.4. Thermal ellipsoid plot of 4-dimethylamino-2,6-*bis*(hydroxymethyl)pyridinium chloride hemihydrate.

H_3(pydim-Cl)Cl and [H_3(pydim-NMe_2)Cl]$_2$(H_2O) are essentially planar. (See the C(1) – C(2) – C(3) – X (X = Cl or $N(CH_3)_2$) torsion angles given in Table 3.1.) Likewise, the pyridine rings in the two previous X-ray studies of 4-dimethylaminopyridinium chloride were also found to be planar, and the pyridine ring in 4-chloropyridinium chloride is also planar.

Table 3.1. Selected X-ray Bond Lengths (Å), Bond Angles (°), and Torsion Angles (°) for H_3(pydim-Cl)Cl and [H_3(pydim-$N(CH_3)_2)^+Cl^-$]$_2$(H_2O).

	H_3(pydim-Cl)Cl	[H_3(pydim-$N(CH_3)_2)^+Cl^-$]$_2$(H_2O)
N(1) – H	0.858(2)	0.859(3)
N(1) – C(1)	1.359(2)	1.355(3)
C(1) – C(6)	1.505(2)	1.514(3)
C(6) – O(1)	1.412(2)	1.423(3)
C(1) – C(2)	1.374(2)	1.361(3)
C(2) – C(3)	1.393(2)	1.425(3)
C(3) – X	1.725(1) (X = Cl)	1.340(3) (X = $N(CH_3)_2$)
N(2) – C(8)		1.461(3)
N(1) – C(1) – C(6)	117.4(1)	115.8(2)
C(1) – C(6) – O(1)	110.9(1)	111.4(2)
C(6) – C(1) – C(2)	123.5(1)	123.5(2)
C(2) – C(3) – X	119.3(1)	121.5(2)
C(2) – C(3) – C(4)	121.7(1)	117.2(2)
C(3) – N(2) – C(8)		121.3(2)
C(8) – N(2) – C(9)		116.7(2)
C(3) – N(2) – C(9)		121.9(2)
N(1) – C(1) – C(6) – O(1)	177.5(1)	26.3(2)
N(1) – C(5) – C(7) – O(2)	13.2(1)	161.3(2)
C(1) – C(2) – C(3) – X	178.7(1) (X = Cl)	178.7(2) (X = $N(CH_3)_2$)
C(2) – C(3) – N(2) – C(8)		0.75(2)
C(4) – C(3) – N(2) – C(9)		5.1(1)

With the exception of the [N(1) – H] bond distances, all the bond lengths and bond angles in [H_3(pydim-NMe_2)Cl]$_2$(H_2O) are very similar to those in the structures of 4-dimethylaminopyridinium chloride dihydrate, anhydrous 4-dimethylaminopyridinium

chloride, and the cyclophane derivative with the 4-dimethylamino-2,6-pyridinedimethanolato moiety. The [N(1) – H] bond distances in H_3(pydim-Cl)Cl and [H_3(pydim-NMe_2)Cl]$_2$(H_2O) are 0.858(2) and 0.859(3) Å, respectively. These distances are somewhat shorter than those reported for 4-dimethylaminopyridinium chloride dihydrate (1.02(3) and 1.09(4) Å), but comparable with the [N – H] bond distance in 4-chloropyridinium chloride (0.873 Å).

As was observed in the two previous X-ray studies of 4-dimethylaminopyridinium chloride and in the structure of the 4-dimethylamino-2,6-pyridinedimethanolato moiety of the cyclophane derivative, the dimethylamino group in H_3(pydim-NMe_2)$^+$ is trigonal planar, and the N(2) – C(3) bond length (1.340(3) Å) is shorter than the sum of the single bond covalent radii for carbon and nitrogen (1.47 Å) [25] and shorter than the N(2) – C(methyl) bond lengths, 1.461(3) Å and 1.462(3) Å. These observations imply a π interaction between the dimethylamino group and the pyridine ring. In contrast, it is worthwhile to note that the C(3) – Cl(1) bond distance (1.7245(14) Å) in H_3(pydim-Cl)$^+$ is very close to the sum of the single bond covalent radii for carbon and chlorine (1.76 Å), implying that there is little or no π interaction between the chlorine atom and the pyridine ring in H_3pydim-Cl^+. The C – Cl bond distance in H_3(pydim-Cl)$^+$ is similar to that in 4-chloropyridinium chloride (1.730 Å).

Hydrogen bonds, observed in the structures of both H_3(pydim-Cl)Cl and [H_3(pydim-NMe_2)Cl]$_2$(H_2O), are summarized in Table 3.2. The pyridinium nitrogen atom in H_3(pydim-Cl)Cl is hydrogen-bonded to the chloride ion, and the pyridinium

nitrogen atom in $[H_3(pydim\text{-}NMe_2)Cl]_2(H_2O)$ is hydrogen-bonded to the water molecule. Moreover, hydrogen bonds between oxygen atoms and chloride ions are found in both structures. For reference, the sums of the van der Waals radii for [N · · · Cl], [N · · · O], and [O · · · Cl] are 3.29 Å, 2.96 Å, and 3.25 Å respectively [25]. The dimethylamino nitrogen atom in $[H_3(pydim\text{-}NMe_2)Cl]_2(H_2O)$ does not engage in hydrogen bonding at all. Short van der Waals contacts are also observed in both structures. For instance, the O(1) · · · Cl(1) distance in the unit cell of $H_3(pydim\text{-}Cl)Cl$ is 3.268 Å, and the distance

Table 3.2. Distances (Å) between Atoms Linked by Hydrogen Bonds in $H_3(pydim\text{-}Cl)Cl$ and $H_3(pydim\text{-}N(CH_3)_2)^+Cl^-$.

Structure	Atoms	D · · · A Distance	Bond Angle
$H_3(pydim\text{-}Cl)Cl$	O(2) – H · · · Cl(2)	3.045 Å	172.71°
	N(1) – H · · · Cl(2)	3.219 Å	159.09°
	O(1) – H · · · Cl(2)	3.158 Å	169.21°
$H_3(pydim\text{-}N(CH_3)_2)^+Cl^-$	O(3) – H · · · Cl(1)	3.194 Å	176.98°
	N(1) – H · · · O(3)	2.867 Å	125.52°
	O(1) – H · · · Cl(1)	3.112 Å	165.11°
	O(2) – H · · · Cl(1)	3.090 Å	163.65°

between two neighboring Cl(1) atoms bonded to separate pyridine rings is 3.428 Å. (The sum of the van der Waals radii for [Cl · · · Cl] is 3.58 Å.) For comparison, the [Cl · · · Cl] distance (3.3352(14) Å) in the unit cell of 4-chloropyridinium chloride was also found to be within the sum of the van der Waals radii.

3.4 Experimental Details

All reactions were carried out open to air, using deionized water as the solvent. Infrared spectra were recorded as KBr pellets on a Nicolet Magna−IR 560 spectrometer,

and the data are reported in cm^{-1}. ^{1}H, ^{13}C, and ^{51}V NMR spectra were obtained at room temperature on a Varian Mercury 300 MHz FTNMR spectrometer at the frequencies 300.068 MHz, 75.452 MHz, and 78.85 MHz, respectively. ^{1}H and ^{13}C chemical shifts are reported in parts per million and were referenced externally with respect to a D_2O solution of $NaOOCCH_2CH_2Si(CH_3)_3$; the protons in the methyl groups are set at $\delta = 0$ in the ^{1}H NMR spectrum and the carbon atoms in the methyl groups are set at $\delta = 0$ in the ^{13}C NMR spectrum. ^{51}V chemical shifts are reported in parts per million and were referenced externally with respect to neat $VOCl_3$ ($\delta = 0$ ppm). UV-vis absorption data were obtained using a Hewlett-Packard Model 8453 spectrometer. Elemental analyses were carried out by Atlantic Microlab, Inc. (Norcross, GA). Melting points were measured using a Mel-Temp 3.0 melting point apparatus. 4-chloro-2,6-pyridinedimethanol and 4-dimethylamino-2,6-pyridinedimethanol [26 – 28, 23], and $Na[VO_2(pydim)] \cdot 4\ H_2O$ [18] were prepared according to published procedures. $Na[VO_2(dipic)]$ was prepared by a method similar to that for preparing $NH_4[VO_2(dipic)]$ [29]. $NaVO_3$, 2,6-dipicolinic acid, and 2,6-pyridinedimethanol were purchased from commercial suppliers and were used as received, without further purification.

3.4.1 Synthesis of $Na[VO_2(dipic)]$

A mixture of $NaVO_3$ (0.729 g, 5.98 mmol) and 2,6-dipicolinic acid (0.999 g, 5.98 mmol) in deionized water (20 mL) was stirred at 80°C for 10 minutes. The pale yellow homogeneous mixture was cooled to room temperature and set aside, open to air, for several days. The product precipitated from solution as a white microcrystalline solid.

Yield = 1.560 g (96 %). Anal. Calc. for $C_7H_3NNaO_6V$: C, 31.02%; H, 1.12%; N, 5.17%. Found: C, 31.01%; H, 1.14%; N, 5.15%. IR data: 3447 (m), 3095 (s), 3058 (m), 1670 (vs), 1600 (s), 1475 (m), 1432 (s), 1370 (vs), 1355 (vs), 1297 (w), 1271 (m), 1221 (w), 1188 (s), 1151 (s), 1074 (vs), 1034 (s), 963 (vs), 929 (s), 861 (m), 830 (m), 805 (w), 781 (s), 747 (s), 685 (s), 676 (s), 594 (m), 564 (w), 457 (s), 438 (m). ^{1}H NMR (D_2O): 8.32 (d, $^3J_{H-H}$ = 7.8 Hz, 2 H), 8.65 (t, $^3J_{H-H}$ = 7.8 Hz, 1 H). ^{13}C NMR (D_2O): 129.9 (? C), 149.9 (? C), 150.8 (? C), 199.1 (2 C). ^{51}V NMR (D_2O): -532.

3.4.2 Synthesis of Na[VO_2(pydim-Cl)] · 2 H_2O

A mixture of $NaVO_3$ (0.070 g, 0.57 mmol) and 4-chloro-2,6-pyridinedimethanol (0.099 g, 0.57 mmol) in deionized water (5 mL) was stirred at 85°C for 3 hours. The volatile components were removed under reduced pressure, leaving a white solid. Yield = 0.156 g. ^{1}H NMR spectroscopy revealed the product to be a mixture, two components of which were $NaVO_2$(pydim-Cl) · 2 H_2O and 4-chloro-2,6-pyridinedimethanol. Anal. Calc. for $C_7H_{10}ClNNaO_4V$: C, 26.82%; H, 3.21%; N, 4.47%. Found: C, 26.79%; H, 3.06%; N, 4.41%. IR data: 3095 (m), 2912 (w), 1590 (s), 1569 (m), 1439 (w), 1410 (m), 1384 (m), 1366 (w), 1305 (w), 1275 (w), 1109 (m), 1084 (s), 1063 (m), 1029 (m), 1009 (w), 998 (m), 916 (m, br), 871 (s), 862 (m), 569 (s, br), 466 (w). ^{1}H NMR (D_2O): 5.46 (s, 4 H), 7.52 (s, 2 H). ^{13}C{^{1}H} NMR (D_2O): 74.9 (2 C), 118.5 (2 C), 149.2 (2 C), 166.7 (1 C). ^{51}V NMR (D_2O): -516.

3.4.3 Synthesis of $Na[VO_2(pydim\text{-}NMe_2)] \cdot 3\ H_2O$

A mixture of $NaVO_3$ (0.119 g, 0.978 mmol) and 4-dimethylamino-2,6-pyridinedimethanol (0.179 g, 0.981 mmol) in deionized water (20 mL) was stirred at 80°C for 3 hours. The mixture was cooled to room temperature and filtered. The filtrate was set aside for 9 days at room temperature and open to air, and the product precipitated as a white microcrystalline solid. The product was isolated and air-dried. Yield = 0.035 g (12%). Anal. Calc. for $C_9H_{18}N_2NaO_7V$: C, 31.78%; H, 5.33%; N, 8.23%. Found: C, 31.46%; H, 5.15%; N, 7.78%. IR data: 3409 (vs), 2921 (m), 2878 (m), 2851 (m), 2822 (m), 1630 (vs), 1541 (m), 1440 (m), 1393 (m), 1341 (w), 1227 (w), 1159 (w), 1085 (m), 1050 (s), 914 (vs), 864 (w), 832 (w), 816 (w), 698 (w), 599 (w), 579 (w), 544 (m), 506 (m). ^1H NMR (D_2O): 2.95 (s, 6 H), 5.28 (s, 4 H), 6.40 (s, 2 H). $^{13}C\{^1H\}$ NMR (D_2O): 41.8 (2 C), 77.3 (2 C), 100.9 (2 C), 160.2 (2 C), 167.5 (1 C). ^{51}V NMR (D_2O): -506.

3.4.4 Synthesis of 4-chloro-2,6-bis(hydroxymethyl)pyridinium chloride

A white suspension of 4-chloro-2,6-pyridinedimethanol (0.258 g, 1.5 mmol) in deionized water (5 mL) was titrated with a 0.110 M HCl solution (27.1 mL, 3.0 mmol). The mixture was stirred 30 minutes at room temperature and filtered. The volatile components of the filtrate were removed *in vacuo*, leaving analytically pure white microcrystals. Yield = 0.274 g (88%). The product was recrystallized from deionized water, yielding the colorless needles used in the X-ray analysis. Anal. Calc. for $C_7H_9Cl_2NO_2$: C, 40.03%; H, 4.32%; N, 6.67%. Found: C, 40.04%; H, 4.29%; N, 6.64%. Melting point = 128.7°C without decomposition. IR data: 3313 (s), 3239 (s),

3095 (m), 3019 (s), 2921 (s), 2893 (s), 2815 (s), 2684 (m), 2520 (m), 2160 (w), 1943 (w), 1889 (w), 1621 (vs), 1489 (w), 1448 (m), 1429 (m), 1415 (m), 1384 (w), 1358 (m), 1345 (m), 1263 (m), 1217 (m), 1178 (w), 1118 (s), 1083 (s), 1011 (w), 984 (m), 949 (w), 893 (m), 863 (m), 805 (w), 666 (m), 615 (w), 591 (w), 539 (w), 485 (w), 472 (w), 435 (w), 418 (w). ^{1}H NMR (D_2O): 4.98 (s, 4 H); 7.97 (s, 2 H). $^{13}C\{^{1}H\}$ NMR (D_2O): 62.3; 126.1; 157.8; 159.5.

3.4.5 Synthesis of 4-dimethylamino-2,6-bis(hydroxymethyl)pyridinium chloride hemihydrate

A white suspension of 4-dimethylamino-2,6-pyridinedimethanol (0.147 g, 0.81 mmol) in deionized water (5 mL) was titrated with a 0.110 M HCl solution (14.8 mL, 1.62 mmol). The mixture was stirred 30 minutes at room temperature and filtered. The volatile components of the filtrate were removed *in vacuo*, leaving white microcrystals. Yield = 0.156 g (89%). The product was recrystallized from deionized water, yielding the colorless needles used in the X-ray analysis. Anal. Calc. for $C_{18}H_{32}Cl_2N_4O_5$: C, 47.48%; H, 7.08%; N, 12.30%. Found: C, 47.39%; H, 7.04%; N, 12.23%. Melting point = 191.8°C without decomposition. IR data: 3262 (vs), 2938 (m), 2836 (m), 2621 (w), 1647 (vs), 1558 (s), 1446 (m), 1434 (m), 1415 (m), 1400 (m), 1356 (m), 1337 (w), 1261 (w), 1229 (m), 1166 (m), 1091 (s), 1079 (s), 1064 (m), 1022 (s), 990 (w), 971 (w), 953 (w), 885 (w), 863 (m), 842 (s), 802 (w), 767 (w), 714 (w), 698 (w), 616 (m), 569 (m), 522 (w), 461 (w), 436 (w). ^{1}H NMR (D_2O): 3.22 (s, 6 H); 4.74 (s, 4 H); 6.78 (s, 2 H). $^{13}C\{^{1}H\}$ NMR (D_2O): 42.3; 62.5; 105.7; 154.1; 160.1.

3.4.6 X-Ray Diffraction Studies

Colorless needles of 4-chloro-2,6-*bis*(hydroxymethyl)pyridinium chloride and 4-dimethylamino-2,6-*bis*(hydroxymethyl)pyridinium chloride hemihydrate were obtained from aqueous solutions at room temperature. The needle-shaped crystals were cut into blocks, and the blocks (0.20 x 0.15 x 0.10 mm^3 for the chloro derivative, and 0.20 x 0.20 x 0.20 mm^3 for the dimethylamino derivative) were mounted on a Cryoloop with Paratone oil. X-ray diffraction data were collected at 100 K for the chloro derivative and at 208 K for the dimethylamino derivative on a Bruker CCD platform diffractometer (Mo Kα (λ = 0.71073 Å)). The SMART [30] program package was used to determine the unit cell parameters and for data collection. The data were processed using SAINT [31] and SADABS [32] to yield the reflection data files. Crystal data and data collection and refinement parameters are summarized in Table A2. The structures, solved by using direct methods and standard difference map techniques, were refined by full-matrix least-squares of F^2 with SHELXTL (Version 6.12) [33]. All hydrogen atoms were included in calculated positions.

3.4.7 Density Functional Theory (DFT) Calculations

The structures of $[VO_2(pydim\text{-}X)]^-$ (X = H, Cl, NMe_2) and $[VO_2(dipic)]^-$ were optimized for the singlet state using the DFT method in the GAUSSIAN 03 program [34], with the LANL2MB basis set [35] and B3LYP functional [36, 37] in the gas phase. Vibrational calculations were completed without solvent interactions, and no negative frequencies were found.

3.5 Conclusion

The research conducted in this chapter indicates that ligands which are better electron donors bind more readily to vanadium. In competition experiments ^{1}H NMR spectroscopy reveals that Me_2N-pydim ligand binds to vanadium(V) more readily than does the pydim ligand, which binds to vanadium(V) more readily than does the Cl-pydim ligand. DFT calculations indicate that Me_2N-pydim is a greater electron donor than pydim which is a better electron donor than Cl-pydim. This observation could be influential in designing stable vanadium based insulin mimetic drugs.

3.6 Supplementary Material

Crystallographic data for the reported structures in this article have been deposited with Cambridge Crystallographic Data Centre as CCDC 663220 (4-chloro-2,6-*bis*(hydroxymethyl)pyridinium chloride) and CCDC 663221 (4-dimethylamino-2,6-*bis*(hydroxymethyl)pyridinium chloride hemihydrate). These data can be obtained free of charge at www.ccdc.camb.ac.uk/const/retrieving.html or from the Cambridge Crystallographic Data Centre, 12, Union Road, Cambridge CB2 1EZ, UK; email: deposit@ccdc.camb.ac.uk; fax: +44(0)1223-336408.

3.7 References

1. T. Ghosh, S. Bhattacharya, A. Das, G. Mukherjee, M. G. B. Drew, Inorg. Chim. Acta 358 (2005) 989.
2. S. Gao, L. H. Huo, X. F. Zhang, S. W. Ng, Acta Cryst. E 61 (2005) 738.
3. A. Pohlmann, S. Nica, T. K. K. Luong, W. Plass, Inorg. Chem. Commun. 8 (2005) 289.
4. M. R. Maurya, S. Agarwal, C. Bader, D. Rehder, Eur. J. Inorg. Chem. (2005) 147-57. M. R. Maurya, S. Agarwal, C. Bader, D. Rehder, Eur. J. Inorg. Chem. (2005) 981.
5. M. R. Maurya, S. Agarwal, C. Bader, M. Ebel, D. Rehder, Dalton Trans. (2005) 537.
6. P. Noblía, M. Vieites, B. S. Parajón-Costa, E. J. Baran, H. Cerecetto, P. Draper, M. González, O. E. Piro, E. E. Castellano, A. Azqueta, J. Inorg. Biochem. 99 (2005) 443.
7. T. Ghosh, C. Bandyopadhyay, S. Bhattacharya, G. Mukherjee, Trans. Met. Chem. 29 (2004) 444.
8. R. S. Ghadwal, M. Sharma, A. Singh, R. C. Mehrotra, Trans. Met. Chem. 29 (2004) 419.
9. R. Ando, H. Inden, M. Sugino, H. Ono, D. Sakaeda, T. Yagyu, M. Maeda, Inorg. Chim. Acta 357 (2004) 1337.
10. M.-J. Xie, Y.-S. Ping, L.-D. Zheng, J.-Z. Hui, C. Peng, Acta Cryst. E60 (2004) m1382.

11. L.-H. Huo, S. Gao, J.-W. Liu, J. Li, S. W. Ng, Acta Cryst. E60 (2004) m758-m760.

12. P. Plitt, H. Pritzkow, R. Krämer, Dalton Trans. (2004) 2314.

13. K. I. Smith, L. L. Borer, M. M. Olmstead, Inorg. Chem. 42 (2003) 7410.

14. D. C. Crans, J. Inorg. Biochem. 80 (2000) 123.

15. D. C. Crans, L. Yang, T. Jakusch, T. Kiss, Inorg. Chem. 39 (2000) 4409.

16. D. C. Crans, M. Mahroof-Tahir, M. D. Johnson, P. C. Wilkins, L. Yang, K. Robbins, A. Johnson, J. A. Alfano, M. E. Godzala III, Inorg. Chim. Acta 356 (2003) 365.

17. D. C. Crans, L. Yang, J. A. Alfano, L.-H. Chi, W. Jin, M. Mahroof-Tahir, K. Robbins, M. M. Toloue, L. K. Chan, A. J. Plante, R. Z. Grayson, G. R. Willsky, Coord. Chem. Rev. 237 (2003) 13.

18. R. J. Fites, A. T. Yeager, T. L. Sarvela, W. A. Howard, G. Zhu, K. Pang, Inorg. Chim. Acta 359 (2006) 248.

19. J. Selbin, L. H. Holmes Jr., S. P. McGlynn, J. Inorg. Nucl. Chem. 25 (1963) 1359.

20. Z. N. Pickett, W. A. Howard, C. R. Graves, J. Chem. Crystallogr. 38 (2008) 717.

21. M. Chao, E. Schempp, D. Rosenstein, Acta Cryst. B33 (1977) 1820.

22. G. L. Bryant Jr., J. A. King Jr., Acta Cryst. C48 (1992) 2036.

23. M. Hashizume, S. Tobey, V. M. Lynch, E. V. Anslyn, Supramolecular Chem. 14 (2002) 511.

24. M. Freytag, P. G. Jones, B. Ahrens, A. K. Fischer, New J. Chem. 23 (1999) 1137.

25. L. Pauling, The Nature of the Chemical Bond, 3rd Edn. (1960) Cornell University Press, New York.

26. A. Suga, T. Sugiyama, M. Otsuka, M. Ohno, Y. Sugiura, K. Maeda, Tetrahedron 47 (1991) 1191.

27. U. Lüning, R. Baumstark, M. Müller, Liebigs Ann. Chem. (1991) 987.

28. S. Bhattacharya, K. Snehalatha, S. K. George, J. Org. Chem. 63 (1998) 27.

29. K. Wieghardt, Inorg. Chem. 17 (1978) 57.

30. Bruker Analytical X-Ray Systems Inc. SMART Software Users Guide, Version 5.1 (1999) Madison, Wisconsin, USA.

31. Bruker Analtyical X-Ray Systems Inc. SAINT Software Users Guide, Version 6.0 (1999) Madison, Wisconsin, USA.

32. Sheldrick GM (2002) SADABS, Version 2.10. Bruker Analytical X-Ray Systems Inc., Madison.

33. Sheldrick GM (2001) SHELXTL, Version 6.12. Bruker Analytical X-Ray Systems Inc., Madison.

34. M. J. Frisch, G. W. Trucks, H. B. Schlegel, G. E. Scuseria, M. A. Robb, J. R. Cheeseman, J. A. Montgomery Jr., T. Vreven, K. N. Kudin, J. C. Burant, J. M. Millam, S. S. Iyengar, J. Tomasi, V. Barone, B. Mennucci, M. Cossi, G. Scalmani, N. Rega, G. A. Petersson, H. Nakatsuji, M. Hada, M. Ehara, K. Toyota, R. Fukuda, J. Hasegawa, M. Ishida, T. Nakajima, Y. Honda, O. Kitao, H. Nakai, M. Klene, X. Li, J. E. Knox, H. P. Hratchian, J. B. Cross, C. Adamo, J. Jaramillo, R. Gomperts, R. E. Stratmann, O. Vazyev, A. J. Austin, R. Cammi, C. Pomelli, J.

W. Ochterski, P. Y. Ayala, K. Morokuma, G. A. Voth, P. Salvador, J. J. Dannenberg, V. G. Zakrzewski, S. Dapprich, A. D. Daniels, M. C. Strain, O. Farkas, D. K. Malick, A. D. Rabuck, K. Raghavachari, J. B. Foresman, J. V. Ortiz, Q. Cui, A. G. Baboul, S. Clifford, J. Cioslowski, B. B. Stefanov, G. Liu, A. Liashenko, P. Piskorz, I. Komaromi, R. L. Martin, D. J. Fox, T. Keith, M. A. Al-Laham, C. Y. Peng, A. Nanayakkara, M. Challacombe, P. M. W. Gill, B. Johnson, W. Chen, M. W. Wong, C. Gonzalez, J. A. Pople, GAUSSIAN 03, Revision B.03, Gaussian, Inc., Pittsburgh, PA, 2003.

35. P. J. Hay, W. R. Wadt, J. Chem. Phys. 82 (1985) 299.

36. A. D. Becke, J. Chem. Phys. 98 (1993) 5648.

37. C. Lee, W. Yang, R. G. Parr, Phys. Rev. B 37 (1988) 785.

Chapter 4 Future Work

Since 1899 it has been known that vanadium salts can be used to treat diabetic patients. Though many compounds have been made, vanadium toxicity has prevented the widespread use of these potential drugs. With increased knowledge on how vanadium builds up in the bone and organ tissues of the body, it is clear that a molecule that is stable under physiological conditions is a key to preventing this toxicity.

Future research should be aimed at evaluating the proposed vanadium mimetic compounds stability in the presence of the ttha-transferrin model presented in Chapter 1. By evaluating the stability of proposed compounds in the presence of the ttha-transferrin model, vanadium toxicity associated with mimetic compound may further elucidated. Compounds which remain intact in the presence of ttha are theorized to result in less vanadium toxicity at physiological conditions. This may also reveal whether vanadium dissociation from a ligand is crucial for an effective vanadium insulim mimetic compound. If the dissociation is crucial vanadium build up in the body might not be preventable.

Based on the research in Chapter 2 the Howard research group is further evaluating the ligands presented in this Thesis. These studies are aimed at evaluating ligand stabilities ensuring a constant pH. Ideally the long term goal of this research is to develop stable vanadium mimetic compounds which could one day have medicinal uses. Once stable vanadium compounds are developed next step will be to submit these compounds for *in vivo* studies.

Appendix

Table A1. Crystal Data and Structure Refinement for $Na_2[(VO)_2(ttha)] \cdot 8\ H_2O$.

Molecular formula	$C_{18}\ H_{40}\ N_4\ Na_2\ O_{22}\ V_2$	
Formula weight	812.39 g mol^{-1}	
Temperature	125(2) K	
Wavelength	0.71073 Å	
Crystal system	Triclinic	
Space group	P-1	
Unit cell dimensions	a = 6.696(3) Å	α = 69.988(5)°
	b = 10.052(4) Å	β = 79.368(6)°
	c = 13.205(5) Å	γ = 70.648(5)°
Volume	785.4(5) $Å^3$	
Z	1	
Density (calculated)	1.718 Mg/m^3	
Absorption coefficient	0.720 mm^{-1}	
F(000)	420	
Crystal size	0.10 x 0.10 x 0.05 mm^3	
Theta range for data collection	1.65 to 30.79°	
Index ranges	$-9 \leq h \leq 9$, $-13 \leq k \leq 14$, $0 \leq l \leq 18$	
Reflections collected	23433	
Independent reflections	[R(int) = 0.1863]	
Completeness to theta = 30.79°	99.0%	
Absorption correction	Empirical/TWINABS	
Max. and min. transmission	0.9649 and 0.9315	
Refinement method	Full-matrix least-squares on F^2	
Number of parameters	240	
Goodness-of-fit on F^2	1.102	
Final R indices [I>2sigma(I)]	R1 = 0.0848, wR2 = 0.1544	
R indices (all data)	R1 = 0.2617, wR2 = 0.2522	
Largest diff. peak and hole	1.061 and -1.292 e.$Å^{-3}$	

Table A2. DFT Calculated Coordinates and Total Energy for $[(VO)_2ttha]^{2-}$ Using LANL2MB Basis Set and B3LYP Functional

wgt	x	y	Z
23	-3.767464	-0.186240	-1.012066
8	-4.081762	-1.972060	-0.434039
6	-3.170030	-2.770077	0.167552
6	-1.729715	-2.059078	0.268573
7	-1.909097	-0.534426	0.238707
6	-2.087226	0.000000	1.668813
6	-3.543840	-0.223978	2.182742
7	-4.507727	0.403273	1.204860
6	-5.907733	-0.172282	1.255537
6	-6.567647	0.022541	-0.206131
8	-5.638741	0.057095	-1.195623
8	-7.813922	0.123189	-0.371619
1	-6.530250	0.303184	2.044586
1	-5.823137	-1.254433	1.459571
6	-4.526912	1.920854	1.322662
6	-3.690799	2.580391	0.111568
8	-3.449079	1.690352	-0.874993
8	-3.330309	3.790287	0.130965
1	-4.121484	2.245451	2.303253
1	-5.576657	2.260100	1.247798
1	-3.763723	-1.304355	2.232736
1	-3.632628	0.208079	3.205417
1	-1.370242	-0.498327	2.357704
1	-1.871934	1.077566	1.641303
6	-0.675741	0.136994	-0.392101
6	0.672397	-0.092688	0.393978
7	1.913075	0.544622	-0.257707
23	3.767264	0.226212	1.007760
8	3.303671	0.531261	2.505934
8	5.635775	-0.028290	1.204115
6	6.566285	-0.041300	0.215635
6	5.910317	0.103990	-1.253541
7	4.504233	-0.454639	-1.183665
6	3.548781	0.146231	-2.186082
6	2.088716	-0.037247	-1.667686
1	1.860699	-1.115355	-1.602337
1	1.379568	0.439794	-2.375982
1	3.634121	-0.324970	-3.191628
1	3.781185	1.221386	-2.276380
6	4.507297	-1.975628	-1.244703
6	3.665530	-2.580571	0.000000
8	3.294261	-3.787056	0.018004
8	3.431666	-1.651055	0.942284
1	5.553440	-2.323179	-1.158228
1	4.097255	-2.332249	-2.212149
1	5.837028	1.178387	-1.498705
1	6.529006	-0.407522	-2.022801
8	7.811249	-0.148206	0.386962

8	4.099461	1.984516	0.360349
6	3.195607	2.767826	-0.271829
6	1.747864	2.068720	-0.342285
1	1.164043	2.384585	0.540876
1	1.202350	2.359344	-1.263327
8	3.409201	3.918310	-0.739458
1	0.896501	-1.168021	0.491940
1	0.612020	0.338198	1.406354
1	-0.606655	-0.267784	-1.414530
1	-0.914566	1.211148	-0.464355
1	-1.139820	-2.337071	-0.623235
1	-1.184693	-2.378116	1.180410
8	-3.371187	-3.940806	0.588075
8	-3.303928	-0.428322	-2.521691

Total Energy
-2089.58696197 Hartree

Table A3. Atomic Coordinates and Thermal Tensors for $Na_2[(VO)_2(ttha)] \cdot 8\ H_2O$.

Atom	x	y	z	U
V	-0.3657(2)	0.79633(15)	0.18887(12)	0.0153(4)
O1	-0.5477(9)	0.9399(6)	0.1332(5)	0.0227(13)
O2	-0.3443(9)	0.6561(6)	0.1078(5)	0.0190(13)
O3	-0.2344(10)	0.6105(7)	-0.0501(5)	0.0296(15)
O4	-0.2889(9)	0.8903(6)	0.2832(5)	0.0186(12)
O5	-0.1600(10)	0.8674(6)	0.4344(5)	0.0240(14)
O6	-0.5278(9)	0.6784(6)	0.3096(4)	0.0178(12)
O7	-0.5456(9)	0.4521(6)	0.4064(5)	0.0220(13)
N1	-0.0871(11)	0.8241(7)	0.0816(5)	0.0158(14)
N2	-0.1117(10)	0.6071(7)	0.2897(5)	0.0147(14)
C1	-0.0938(12)	0.9853(8)	0.0397(6)	0.0156(16)
H1A	-0.0970	1.0202	0.1018	0.019
H1B	-0.2268	1.0434	0.0038	0.019
C2	-0.0923(13)	0.7718(9)	-0.0117(7)	0.0187(17)
H2A	0.0540	0.7192	-0.0336	0.022
H2B	-0.1468	0.8586	-0.0740	0.022
C3	-0.2304(13)	0.6699(9)	0.0165(7)	0.0188(17)
C4	0.1056(13)	0.7331(8)	0.1429(7)	0.0175(17)
H4A	0.1283	0.7871	0.1879	0.021
H4B	0.2321	0.7174	0.0912	0.021
C5	0.0795(12)	0.5846(9)	0.2146(7)	0.0183(17)
H5A	0.0667	0.5275	0.1693	0.022
H5B	0.2060	0.5275	0.2560	0.022
C6	-0.0794(13)	0.6521(9)	0.3801(7)	0.0181(17)
H6A	0.0748	0.6270	0.3861	0.022
H6B	-0.1412	0.5952	0.4486	0.022
C7	-0.1792(13)	0.8155(9)	0.3654(7)	0.0180(17)
C8	-0.2040(14)	0.4814(9)	0.3317(7)	0.0221(18)
H8A	-0.1411	0.4131	0.3996	0.027
H8B	-0.1699	0.4261	0.2785	0.027
C9	-0.4431(13)	0.5371(8)	0.3528(7)	0.0166(16)
Na1	-0.5000	1.0000	0.5000	0.0250(11)
Na2	0.0000	1.0000	0.5000	0.0258(11)
O1S	-0.3433(9)	1.1655(6)	0.5245(5)	0.0234(14)
H1SA	-0.3765	1.1779	0.5976	0.050
H1SB	-0.3714	1.2626	0.4678	0.050
O2S	-0.4525(12)	0.8457(7)	0.6848(6)	0.0356(17)
H2SA	-0.542(13)	0.782(8)	0.699(6)	0.050
H2SB	-0.524(14)	0.913(7)	0.728(5)	0.050
O3S	0.0538(14)	1.1294(9)	0.3160(7)	0.051(2)
H3SA	-0.018(13)	1.178(11)	0.251(5)	0.050
H3SB	0.196(7)	1.140(12)	0.295(8)	0.050
O4S	-0.5927(11)	0.6330(7)	0.8564(6)	0.0318(16)
H4SA	-0.486(13)	0.628(10)	0.899(7)	0.050
H4SB	-0.597(16)	0.532(5)	0.876(8)	0.050

Table A4. DFT Calculated Coordinates and Total Energy For [(VO_2) pydim- NMe_2]$^-$ Using LANL2MB Basis Set and B3LYP Functional

wgt	x	y	z
23	0.000000	0.000000	0.000000
7	2.209521	0.000028	0.082449
6	2.884833	-1.192189	0.094217
6	4.289191	-1.231718	0.152359
6	5.017112	0.000097	0.191683
6	4.289110	1.231891	0.152570
6	2.884774	1.192301	0.094414
6	1.799908	2.327305	-0.019450
8	0.542890	1.758568	-0.356425
1	2.133238	3.069090	-0.792993
1	1.765563	2.862013	0.967348
1	4.810773	2.192754	0.151161
7	6.461625	0.000155	0.319524
6	7.178517	-1.252845	-0.091792
1	8.260578	-1.092329	0.047420
1	6.867156	-2.090208	0.555680
1	6.992356	-1.535145	-1.148893
6	7.178571	1.252744	-0.092963
1	8.260596	1.092464	0.046821
1	6.992765	1.533816	-1.150456
1	6.866938	2.090826	0.553435
1	4.810891	-2.192558	0.150759
6	1.800070	-2.327256	-0.019886
8	0.542943	-1.758545	-0.356514
1	1.765887	-2.862340	0.966714
1	2.133398	-3.068719	-0.793738
8	-0.328808	-0.000063	1.611947
8	-1.496556	-0.000039	-0.634282

Total Energy

-822.200955855 Hartree

Table A5. DFT Calculated Coordinates and Total Energy For [(VO_2) pydim]$^-$ Using LANL2MB Basis Set and B3LYP Functional

wgt	x	y	z
23	0.000000	0.000000	0.000000
7	0.079539	2.221252	0.000000
6	0.095042	2.884768	1.199633
6	0.095042	4.297892	1.229751
6	0.091169	4.994613	0.000000
6	0.095042	4.297892	-1.229751
6	0.095042	2.884768	-1.199633
6	0.147179	1.789245	-2.327926
8	0.404506	0.516300	-1.753855
1	0.942249	2.073032	-3.067482
1	-0.838004	1.813628	-2.866052
1	0.108559	4.843478	-2.181895
1	0.101550	6.094394	0.000000
1	0.108559	4.843478	2.181895
6	0.147179	1.789245	2.327926
8	0.404506	0.516300	1.753855
1	-0.838004	1.813628	2.866052
1	0.942249	2.073032	3.067482
8	-1.634692	-0.181872	0.000000
8	0.500004	-1.545811	0.000000

Total Energy

-689.890104373 Hartree

Table A6. DFT calculated coordinates and total energy for $[(VO_2)\ pydim\text{-}Cl]^-$ using LANL2MB Basis Set and B3LYP Functional

wgt	x	y	z
23	0.000000	0.000000	0.000000
7	-2.230033	0.000000	-0.029878
6	-2.888186	1.203624	-0.027288
6	-4.304666	1.250741	0.011331
6	-4.951991	0.000000	0.035876
6	-4.304666	-1.250741	0.011331
6	-2.888186	-1.203624	-0.027288
6	-1.788167	-2.332790	-0.111718
8	-0.531048	-1.751606	-0.403559
1	-2.098052	-3.068948	-0.899969
1	-1.789680	-2.868631	0.875069
1	-4.869348	-2.190750	0.012479
17	-6.887063	0.000000	0.054844
1	-4.869348	2.190750	0.012479
6	-1.788167	2.332790	-0.111718
8	-0.531048	1.751606	-0.403559
1	-1.789680	2.868631	0.875069
1	-2.098052	3.068948	-0.899969
8	1.538453	0.000000	-0.515984
8	0.196900	0.000000	1.630601

Total Energy

-704.244839368 Hartree

Table A7. DFT Calculated Coordinates and Total Energy for [(VO_2) dipic]$^-$ Using LANL2MB Basis Set and B3LYP Functional

wgt	x	y	z
23	0.000000	0.000000	0.000000
7	-2.195062	0.000000	-0.001625
6	-2.867088	1.199687	-0.000971
6	-4.280744	1.226074	0.000374
6	-4.982730	0.000000	0.001021
6	-4.280744	-1.226074	0.000378
6	-2.867088	-1.199687	-0.000968
6	-1.795292	-2.373866	-0.001783
8	-0.548067	-1.838279	-0.002421
8	-2.092394	-3.599686	-0.000807
1	-4.811376	-2.187131	0.000904
1	-6.082774	0.000000	0.002038
1	-4.811376	2.187131	0.000897
6	-1.795292	2.373866	-0.001792
8	-0.548067	1.838279	-0.002429
8	-2.092394	3.599686	-0.000816
8	1.028994	0.000002	1.257399
8	1.038452	-0.000002	-1.249468

Total Energy
-835.875388213 Hartree

Table A8. Crystal, Intensity Collection and Refinement Data For $H_3(pydim\text{-}Cl)^+Cl^-$ and $[H_3(pydim\text{-}N(CH_3)_2)^+Cl^-]_2(H_2O)$

	$H_3(pydim\text{-}Cl)^+Cl^-$	$[H_3(pydim\text{-}N(CH_3)_2)^+Cl^-]_2(H_2O)$
Formula	$C_7H_9Cl_2NO_2$	$C_{18}H_{32}Cl_2N_4O_5$
Formula Weight	210.06	455.38
Space Group	P-1	Aba2
a, Å	6.0651(8)	17.2179(14)
b, Å	8.4393(8)	17.6332(15)
c, Å	8.6554(9)	7.2068(6)
α, °	78.845(1)	90
β, °	83.156(1)	90
γ, °	89.047(1)	90
V, Å^3	431.55(8)	2188.0(3)
Z	2	4
Temperature, K	100(2)	208(2)
ρ (calc), g cm^{-3}	1.616	1.382
μ (Mo, Kα), mm^{-1}	0.708	0.333
Max., Min. trans.	0.9326, 0.8714	0.9363, 0.9363
θ range (deg.)	2.42 – 28.13	2.31 – 28.25
Completeness to θ max (%)	93.6	94.5
Reflections Collected	7277	7089
Unique Collections	1975	2300
Data, restraints, params.	1975/0/115	2300/1/147
R_1, wR_2 (I>2s(I))	0.0274, 0.0665	0.0408, 0.1205
R_1, wR_2 (all data)	0.0337, 0.0699	0.0425, 0.1218
GOF	1.069	1.140
Largest diff. peak, hole (e/Å^{-3})	0.278, – 0.307	0.737, – 0.480

Table A9. Atomic Coordinates and Thermal Tensors for $(H_3pydim\text{-}Cl)^+Cl^-$.

Atom	x	y	z	U
Cl1	0.28197(6)	0.46865(4)	0.40013(5)	0.02165(11)
O2	-0.40922(18)	0.13770(12)	0.07221(13)	0.0198(2)
H5	-0.5084	0.1564	0.0113	0.024
N1	-0.0553(2)	0.09459(15)	0.21769(14)	0.0141(3)
O1	0.37682(18)	-0.15198(13)	0.40340(13)	0.0190(2)
H4	0.4900	-0.1752	0.3464	0.023
C2	0.2280(2)	0.16451(17)	0.35662(17)	0.0154(3)
H2	0.3519	0.1365	0.4138	0.018
C3	0.1491(2)	0.32227(17)	0.33061(17)	0.0163(3)
C7	-0.3164(2)	0.28433(18)	0.08787(18)	0.0176(3)
H13A	-0.4308	0.3495	0.1381	0.021
H13B	-0.2594	0.3470	-0.0179	0.021
C4	-0.0305(2)	0.36564(17)	0.24709(17)	0.0170(3)
H3	-0.0834	0.4735	0.2304	0.020
C6	0.1972(2)	-0.12232(17)	0.31216(18)	0.0154(3)
H6A	0.0720	-0.1953	0.3628	0.019
H6B	0.2428	-0.1455	0.2052	0.019
C1	0.1225(2)	0.05037(17)	0.29755(17)	0.0143(3)
C5	-0.1304(2)	0.24722(17)	0.18878(17)	0.0152(3)
Cl2	0.24142(6)	0.23831(4)	0.84771(4)	0.01853(11)
H1	-0.124(3)	0.023(2)	0.183(2)	0.030(5)

Table A10. Atomic Coordinates and Thermal Tensors for $[(H_3pydim\text{-}NMe_2)^+Cl^-]_2(H_2O)$.

Atom	x	y	z	U
Cl1	0.12290(3)	0.39512(3)	0.38410(14)	0.02961(19)
N1	0.39911(11)	0.57567(10)	0.4169(3)	0.0201(5)
C1	0.33676(12)	0.52954(11)	0.3968(4)	0.0193(5)
C2	0.26339(12)	0.55756(12)	0.4125(4)	0.0201(5)
H2	0.2209	0.5256	0.3970	0.024
C3	0.25174(13)	0.63589(12)	0.4526(4)	0.0188(5)
C4	0.31917(12)	0.68121(13)	0.4794(4)	0.0193(5)
H4	0.3142	0.7323	0.5095	0.023
C5	0.39128(13)	0.64967(13)	0.4609(4)	0.0185(5)
C6	0.35463(14)	0.44632(12)	0.3675(5)	0.0245(6)
H6A	0.3530	0.4202	0.4859	0.029
H6B	0.3153	0.4241	0.2879	0.029
C7	0.46598(13)	0.69355(12)	0.4897(4)	0.0228(5)
H7A	0.5027	0.6619	0.5562	0.027
H7B	0.4884	0.7054	0.3697	0.027
C8	0.11108(14)	0.61875(15)	0.4411(5)	0.0275(7)
H8A	0.1103	0.5985	0.3175	0.033
H8B	0.0655	0.6491	0.4609	0.033
H8C	0.1119	0.5778	0.5290	0.033
C9	0.16776(15)	0.74681(16)	0.4925(6)	0.0335(7)
H9A	0.1752	0.7593	0.6210	0.040
H9B	0.1158	0.7597	0.4563	0.040
H9C	0.2040	0.7748	0.4182	0.040
N2	0.18032(11)	0.66559(11)	0.4654(4)	0.0237(5)
O1	0.42903(10)	0.43607(10)	0.2854(3)	0.0278(4)
H1	0.4239	0.4274	0.1743	0.033
O2	0.45482(11)	0.76131(10)	0.5894(3)	0.0254(4)
O3	0.0000	0.5000	0.1736(5)	0.0302(7)
H2A	0.4357(18)	0.7892(18)	0.520(5)	0.019(8)
H3	0.0277(19)	0.4758(19)	0.226(5)	0.023(9)
H1N	0.4448(18)	0.5562(16)	0.421(5)	0.023(7)